ATLAS NOTE

ATLAS-CONF-2014-009

March 20, 2014
Revision: May 5, 2014

Updated coupling measurements of the Higgs boson with the ATLAS detector using up to 25 fb^{-1} of proton-proton collision data

The ATLAS Collaboration

Abstract

This note is a presentation of an update of the measurements of the signal strengths and couplings of the Higgs boson using the full 2011 and 2012 pp collision data sample recorded by the ATLAS experiment at the LHC at $\sqrt{s}$ = 7 TeV, respectively $\sqrt{s}$ = 8 TeV, for the channels $H \to \gamma\gamma$, $H \to ZZ^* \to 4\ell$, $H \to WW^* \to \ell\nu\ell\nu$ and $H \to b\bar{b}$, and the full 2012 pp collision data sample at $\sqrt{s}$ = 8 TeV for the $H \to \tau\tau$ channel. The combined signal strength is determined to be $\mu = 1.30 \pm 0.12\,\text{(stat)}\,^{+0.14}_{-0.11}\,\text{(sys)}$ at a Higgs boson mass of 125.5 GeV. Evidence for direct decay into fermions is found at the 3.7σ level from the combination of the $H \to b\bar{b}$ and $H \to \tau\tau$ channels with a signal strength of $\mu^{bb,\tau\tau} = 1.09 \pm 0.24\,\text{(stat)}\,^{+0.27}_{-0.21}\,\text{(sys)}$. Measurements of production and decay mode specific signal strengths and Higgs boson coupling determinations in various benchmark models show good agreement with the Standard Model Higgs boson hypothesis.

The coloring scheme of the likelihood contour plot of Figure 5(b) for the VH(bb) channel has been corrected.

1 Introduction

The observation of a new particle in the search for the Standard Model (SM) Higgs boson at the LHC, reported by the ATLAS [1] and CMS [2] Collaborations, is a milestone in the quest to understand electroweak symmetry breaking. Precision measurements of the properties of the new boson are of critical importance. Among its key properties are the couplings to each of the SM fermions and bosons. In Ref. [3] the ATLAS Collaboration reported first measurements of the mass of the particle and its coupling properties using the diboson decay modes to $\gamma\gamma$, ZZ^* and WW^*. In Ref. [4] the CMS Collaboration reported on the first evidence for the direct decay of the Higgs boson to fermions. Since the publication on the diboson channels, the ATLAS Collaboration has made available important results on fermionic channels, namely $H \rightarrow b\bar{b}$ [5] and $H \rightarrow \tau\tau$ [6]. An update of the measurements of the coupling properties of the Higgs boson including the new fermionic modes is presented in this document. The analysis uses the full 2011 and 2012 pp collision data sample recorded by the ATLAS experiment at $\sqrt{s}$ = 7 TeV and $\sqrt{s}$ = 8 TeV, respectively, for the channels $H \rightarrow \gamma\gamma$, $H \rightarrow ZZ^* \rightarrow 4\ell$, $H \rightarrow WW^* \rightarrow \ell\nu\ell\nu$ [3] and $H \rightarrow b\bar{b}$ [5], and the full 2012 pp collision data sample at $\sqrt{s}$ = 8 TeV for the $H \rightarrow \tau\tau$ channel [6].

The results are based on the same statistical model as defined in Refs. [1, 3]. The aspects of the individual channels relevant for these measurements are briefly summarised in Section 2. The statistical procedure and the treatment of systematic uncertainties are outlined in Section 3. In Section 4 the measured yields are analysed in terms of the signal strengths, for different production and decay modes and their combinations. Finally, in Section 5 the couplings of the newly discovered boson are tested through fits to the observed data. These studies aim to probe, under the assumptions described in the text, the Lagrangian structure in the vector boson and fermion sectors, specifically couplings to fermions and bosons, the ratio of couplings to the W and Z bosons, to up- and down-type fermions, to leptons and quarks, and the effective couplings to photons and gluons. A limit is set on the branching ratio to invisible or undetected decay modes. In addition, generic coupling models are explored.

2 Input Channels

The determination of the integrated luminosity for the 2012 dataset has been improved with respect to that of Ref. [3], with a new value of 20.3 fb^{-1} with an uncertainty of 2.8%. This uncertainty is derived, following the same methodology as that detailed in Ref. [7], from a preliminary calibration of the luminosity scale derived from beam-separation scans performed in November 2012. The $H \rightarrow ZZ^* \rightarrow 4\ell$, $H \rightarrow \gamma\gamma$ and $H \rightarrow WW^* \rightarrow \ell\nu\ell\nu$ results are taken from the analysis in Ref. [3], using the full 2011 and 2012 datasets, and taking into account the new luminosity measurement for 2012. The $H \rightarrow b\bar{b}$ and $H \rightarrow \tau\tau$ results, documented in Ref. [5] and Ref. [6], respectively, have been evaluated at the measured mass of 125.5 GeV as obtained from the $H \rightarrow ZZ^* \rightarrow 4\ell$ and $H \rightarrow \gamma\gamma$ [3] channels, resulting in a change of the extracted signal strengths of $2 - 3\%$ caused by the change in the cross sections and branching ratios with respect to the reference mass of 125 GeV used in Refs. [5, 6].

The event selections of the vector boson fusion (VBF) category of the $H \rightarrow WW^* \rightarrow \ell\nu\ell\nu$ analysis in Ref. [3] and the dilepton final state of the $H \rightarrow \tau\tau$ analysis in Ref. [6] have a small overlap. In order to render the two signal selections mutually exclusive for this combination, a cut on the reconstructed ditau invariant mass $m_{\tau\tau} < m_Z - 25$ GeV is added to the $H \rightarrow WW^* \rightarrow \ell\nu\ell\nu$ VBF selection and a cut on $m_{\tau\tau} > m_Z - 25$ GeV is added to the dilepton $H \rightarrow \tau\tau$ selection. For this purpose, $m_{\tau\tau}$ is calculated from the lepton momenta and $E_{\mathrm{T}}^{\mathrm{miss}}$ in the collinear approximation [6]. Application of this cut has no impact on the events in the bins with the best signal-to-background ratio (highest score of the multivariate discriminant) in the $H \rightarrow \tau\tau$ analysis. In the VBF $H \rightarrow WW^* \rightarrow \ell\nu\ell\nu$ analysis the cut removes most of the $H \rightarrow \tau\tau$ signal contamination, but also removes ~10% of the expected VBF $H \rightarrow WW^* \rightarrow \ell\nu\ell\nu$ signal

events. However, these removed $H \to WW^* \to \ell\nu\ell\nu$ signal events are mostly retained within the $H \to \tau\tau$ analysis selection.

The $H \to WW^* \to \ell\nu\ell\nu$ channel also contaminates the $H \to \tau\tau$ selection. In Ref. [6] this was treated as a background, with SM signal strength. In the present study, this contamination is rescaled by the measured $H \to WW^* \to \ell\nu\ell\nu$ signal strength.

The final states and channel categories considered in this analysis are summarised in Table 1.

3   Statistical Procedure

The statistical treatment of the data is described in Refs. [8–12]. Hypothesis testing and confidence intervals are based on the $\Lambda(\alpha)$ profile likelihood ratio [13] test statistic. The latter depends on one or more parameters of interest α, such as the Higgs boson signal strength μ normalised to the SM expectation (so that $\mu = 1$ corresponds to the SM Higgs boson hypothesis and $\mu = 0$ to the background-only hypothesis), Higgs boson mass m_H, coupling strength scale factors κ and their ratios λ, as well as on nuisance

Table 1: Summary of the individual channels entering the combined results presented here. In channels sensitive to associated production of the Higgs boson, V indicates a W or Z boson. The symbols $\otimes$ and $\oplus$ represent direct products and sums over sets of selection requirements, respectively. The abbreviations listed here are described in the corresponding references indicated in the last column. For the $H \to \gamma\gamma$ channel the variables p_{Tt} and η_γ are defined in Ref. [3].

Higgs boson Decay	Subsequent Decay	Sub-Channels	$\int L\,dt$ [fb^{-1}]	Ref.
2011 $\sqrt{s}$ =7 TeV				
$H \to \gamma\gamma$	–	10 categories $\{p_{Tt} \otimes \eta_\gamma \otimes \text{conversion}\} \oplus \{\text{2-jet VBF}\}$	4.8	[3]
$H \to ZZ^*$	4ℓ	$\{4e, 2e2\mu, 2\mu2e, 4\mu, \text{2-jet VBF}, \ell\text{-tag}\}$	4.6	[3]
$H \to WW^*$	$\ell\nu\ell\nu$	$\{ee, e\mu, \mu e, \mu\mu\} \otimes \{\text{0-jet, 1-jet, 2-jet VBF}\}$	4.6	[3]
$VH \to Vbb$	$Z \to \nu\nu$	$E_{\mathrm{T}}^{\mathrm{miss}} \in \{120 - 160, 160 - 200, \geq 200 \text{ GeV}\} \otimes \{\text{2-jet, 3-jet}\}$	4.6	
	$W \to \ell\nu$	$p_{\mathrm{T}}^W \in \{< 50, 50 - 100, 100 - 150, 150 - 200, \geq 200 \text{ GeV}\}$	4.7	[5]
	$Z \to \ell\ell$	$p_{\mathrm{T}}^Z \in \{< 50, 50 - 100, 100 - 150, 150 - 200, \geq 200 \text{ GeV}\}$	4.7	
2012 $\sqrt{s}$ =8 TeV				
$H \to \gamma\gamma$	–	14 categories: $\{p_{Tt} \otimes \eta_\gamma \otimes \text{conversion}\} \oplus$ $\{\text{loose, tight 2-jet VBF}\} \oplus \{\ell\text{-tag}, E_{\mathrm{T}}^{\mathrm{miss}}\text{-tag, 2-jet VH}\}$	20.3	[3]
$H \to ZZ^*$	4ℓ	$\{4e, 2e2\mu, 2\mu2e, 4\mu, \text{2-jet VBF}, \ell\text{-tag}\}$	20.3	[3]
$H \to WW^*$	$\ell\nu\ell\nu$	$\{ee, e\mu, \mu e, \mu\mu\} \otimes \{\text{0-jet, 1-jet, 2-jet VBF}\}$	20.3	[3]
$VH \to Vbb$	$Z \to \nu\nu$	$E_{\mathrm{T}}^{\mathrm{miss}} \in \{120 - 160, 160 - 200, \geq 200 \text{ GeV}\} \otimes \{\text{2-jet, 3-jet}\}$	20.3	
	$W \to \ell\nu$	$p_{\mathrm{T}}^W \in \{<90, 90\text{-}120, 120\text{-}160, 160\text{-}200, \geq 200 \text{ GeV}\} \otimes \{\text{2-jet, 3-jet}\}$	20.3	[5]
	$Z \to \ell\ell$	$p_{\mathrm{T}}^Z \in \{<90, 90\text{-}120, 120\text{-}160, 160\text{-}200, \geq 200 \text{ GeV}\} \otimes \{\text{2-jet, 3-jet}\}$	20.3	
$H \to \tau\tau$	$\tau_{\mathrm{lep}}\tau_{\mathrm{lep}}$	$\{ee, e\mu, \mu\mu\} \otimes \{\text{boosted, 2-jet VBF}\}$	20.3	
	$\tau_{\mathrm{lep}}\tau_{\mathrm{had}}$	$\{e, \mu\} \otimes \{\text{boosted, 2-jet VBF}\}$	20.3	[6]
	$\tau_{\mathrm{had}}\tau_{\mathrm{had}}$	$\{\text{boosted, 2-jet VBF}\}$	20.3	

3

parameters $\boldsymbol{\theta}$,

$$\Lambda(\boldsymbol{\alpha}) = \frac{L(\boldsymbol{\alpha}, \hat{\hat{\boldsymbol{\theta}}}(\boldsymbol{\alpha}))}{L(\hat{\boldsymbol{\alpha}}, \hat{\boldsymbol{\theta}})}. \tag{1}$$

The likelihood functions in the numerator and denominator of the above equation are built using sums of signal and background probability density functions (pdfs) in the discriminating variables. These variables are the $\gamma\gamma$, 4ℓ and $2b$-jet masses for $H\to\gamma\gamma$, $H\to ZZ^*\to 4\ell$ and $H \to b\bar{b}$, respectively, the transverse mass m_{T} (defined in Ref. [3]) for the $H\to WW^*\to \ell\nu\ell\nu$ channel and a multivariate discriminant output distribution for $H \to \tau\tau$. The pdfs are derived from MC simulation for the signal and from both data and simulation for the background. Likelihood fits to the observed data are done for the parameters of interest. The single circumflex in Eq. 1 denotes the unconditional maximum likelihood estimate of a parameter and the double circumflex denotes the conditional maximum likelihood estimate for given fixed values of the parameters of interest $\boldsymbol{\alpha}$.

Systematic uncertainties and their correlations [8] are modelled by introducing nuisance parameters $\boldsymbol{\theta}$ described by likelihood functions associated with the estimate of the corresponding effect. The choice of the parameters of interest depends on the test under consideration, with the remaining parameters being "profiled", i.e., similarly to nuisance parameters they are set to the values that maximise the likelihood function for the given fixed values of the parameters of interest.

Asymptotically, a test statistic $-2\ln\Lambda(\boldsymbol{\alpha})$ of several parameters of interest $\boldsymbol{\alpha}$ is distributed as a χ^2 distribution with n degrees of freedom, where n is the dimensionality of the vector $\boldsymbol{\alpha}$. In particular, the $100(1 - \beta)\%$ confidence level (CL) contours are defined by $-2\ln\Lambda(\boldsymbol{\alpha}) < k_\beta$, where k_β satisfies $P(\chi_n^2 > k_\beta) = \beta$. For two degrees of freedom the 68% and 95% CL contours are given by $-2\ln\Lambda(\boldsymbol{\alpha}) = 2.3$ and 6.0, respectively. All results presented in the following sections are based on likelihood evaluations and therefore give only approximate CL intervals.[1]

For the measurements in the following sections the compatibility with the Standard Model, $\mathrm{p_{SM}}$, is quantified using the p-value obtained from the profile likelihood ratio $\Lambda(\boldsymbol{\alpha} = \boldsymbol{\alpha}_{SM})$, where $\boldsymbol{\alpha}$ is the set of parameters of interest and $\boldsymbol{\alpha}_{SM}$ are their Standard Model values. For a given coupling benchmark model, $\boldsymbol{\alpha}$ is the set of κ_i and λ_{ij} parameters of that model, where the indices i, j refer to the parameters of interest of the model. All other parameters are treated as independent nuisance parameters.

4 Signal Strength in Production and Decay Modes

This section focuses on the measurement of the global signal strength parameter μ and the individual signal strength parameters μ_i^f which depend upon the Higgs boson production mode i and the decay channel f, for a fixed mass hypothesis corresponding to the measured value $m_H = 125.5$ GeV [3]. The parameters μ and μ_i^f are determined from a fit to the data using the profile likelihood ratio $\Lambda(\mu)$ (see Eq. 1).

The results are shown in Fig. 1, where the signal strengths measured in the five individual channels are presented[2]. The signal strength normalised to the SM expectation, obtained by combining the three diboson channels, was published in Ref. [3] as $\mu^{\gamma\gamma,ZZ^*,WW^*} = 1.33 \pm 0.14\,(\mathrm{stat}) \pm 0.15\,(\mathrm{sys})$. With the changes described in Section 2, this value is updated to $\mu^{\gamma\gamma,ZZ^*,WW^*} = 1.35 \pm 0.14\,(\mathrm{stat})\,^{+0.16}_{-0.14}\,(\mathrm{sys})$. The combination of the two fermion channels $H \to b\bar{b}$ and $H \to \tau\tau$ yields a signal strength

$$\mu^{bb,\tau\tau} = 1.09 \pm 0.24\,(\mathrm{stat})\,^{+0.27}_{-0.21}\,(\mathrm{sys}),$$

---

[1]Whenever probabilities are translated into the number of Gaussian standard deviations the two-sided convention is chosen.
[2]The results for $H\to\gamma\gamma$, $H\to ZZ^*\to 4\ell$ and $H \to b\bar{b}$ are taken from the individual analyses, while the results for $H\to WW^*\to \ell\nu\ell\nu$ and $H \to \tau\tau$ are taken from the combination of these two channels with independent signal strengths for the two final states in order to take the signal cross contamination into account (see Section 2).

corresponding to 3.7σ evidence for the direct decay of the Higgs boson into fermions. Finally, the signal strength, obtained by combining all five channels, is:

$$\mu = 1.30 \pm 0.12\,\text{(stat)}\,^{+0.14}_{-0.11}\,\text{(sys)}.$$

A significant component of the systematic uncertainty is associated to the theoretical values of the cross sections and branching ratios. The uncertainty on the cross section amounts to $\pm 7\%$, dominated by uncertainties on the QCD renormalisation and factorisation scales and the parton distribution function (PDF) for the gluon-gluon fusion process (ggF). The uncertainty on the mass measurement of ± 0.6 GeV reported in Ref. [3] leads to a $\pm 3\%$ uncertainty on μ.

The compatibility between this measurement and the SM Higgs boson expectation ($\mu = 1$) is about 7%; the use of a flat likelihood for the ggF QCD scale systematic uncertainty in the quoted $\pm 1\sigma$ interval yields a similar level of compatibility (8%) with the $\mu = 1$ hypothesis. The overall compatibility between the signal strengths measured in the five final states and the SM predictions is about 11%. Both the central value of μ and the SM compatibility have changed little with respect to the diboson measurements of Ref. [3]. The contribution of the diboson channels still dominates the measurement, and the combination of the $H \to b\bar{b}$ and $H \to \tau\tau$ modes has a compatible measured value of μ .

The measurements of the signal strengths described above do not give direct information on the relative contributions of the different production mechanisms. Furthermore, fixing the ratios of the production cross sections for the various processes to the values predicted by the Standard Model may conceal differences between data and theoretical predictions. Therefore, in addition to the signal strengths of different decay channels, the signal strengths of different production processes contributing to the same decay channel[3] are determined, exploiting the sensitivity offered by the use of event categories in the analyses of all the channels.

The data are fitted separating the VBF and VH processes, which involve the Higgs boson coupling to vector bosons, from the ggF and ttH processes, which involve the Higgs boson coupling to fermions (mainly the top-quark).[4] Two signal strength parameters, $\mu^f_{\text{ggF}+ttH} = \mu^f_{\text{ggF}} = \mu^f_{ttH}$ and $\mu^f_{\text{VBF}+VH} = \mu^f_{\text{VBF}} = \mu^f_{VH}$, which scale the SM-predicted rates to those observed, are introduced for the channels $H \to \gamma\gamma$, $H \to ZZ^* \to 4\ell$, $H \to WW^* \to \ell\nu\ell\nu$ and $H \to \tau\tau$ indexed by the parameter f. The $H \to b\bar{b}$ final state is not included, as the current analysis is only sensitive to the VH production mode, and not to the VBF or ggF production modes. The results are shown in Fig. 2. The 95% CL contours of the measurements are consistent with the SM expectation.

A combination of all four channels provides a higher-sensitivity test of the theory. This can be done in a model-independent way (i.e. without assumptions on the Higgs boson branching ratios) by measuring the ratios $\mu_{\text{VBF}+VH}/\mu_{\text{ggF}+ttH}$ for the individual final states and their combination. The result of the fit to the data with the likelihood $\Lambda(\mu_{\text{VBF}+VH}/\mu_{\text{ggF}+ttH})$ is

$$\mu_{\text{VBF+VH}}/\mu_{\text{ggF}+ttH} = 1.4^{+0.5}_{-0.4}\,\text{(stat)}\,^{+0.4}_{-0.2}\,\text{(sys)}.$$

The results for individual channels and their combination are shown in Fig. 3. Good agreement with the SM expectation is observed. The main components of the systematic uncertainty [5] come from the theoretical predictions for the ggF contributions to the various categories and jet multiplicities.

The changes in the results of the $H \to WW^* \to \ell\nu\ell\nu$ and $H \to \tau\tau$ channels, respectively from Ref. [3] and Ref. [6], are mainly due to the separation of their VBF signal regions by the cut on $m_{\tau\tau}$ described in

---

[3]Such an approach avoids model assumptions needed for a consistent parameterisation of production and decay channels in terms of Higgs boson couplings.

[4]Such a separation is possible under the assumption that the kinematic properties of these production modes agree with the SM predictions within uncertainties.

[5]A component of the statistical uncertainty in the results for $\mu_{\text{VBF}+VH}/\mu_{\text{ggF}+ttH}$ in Ref. [3] was incorrectly counted as systematic error there. It is corrected here.
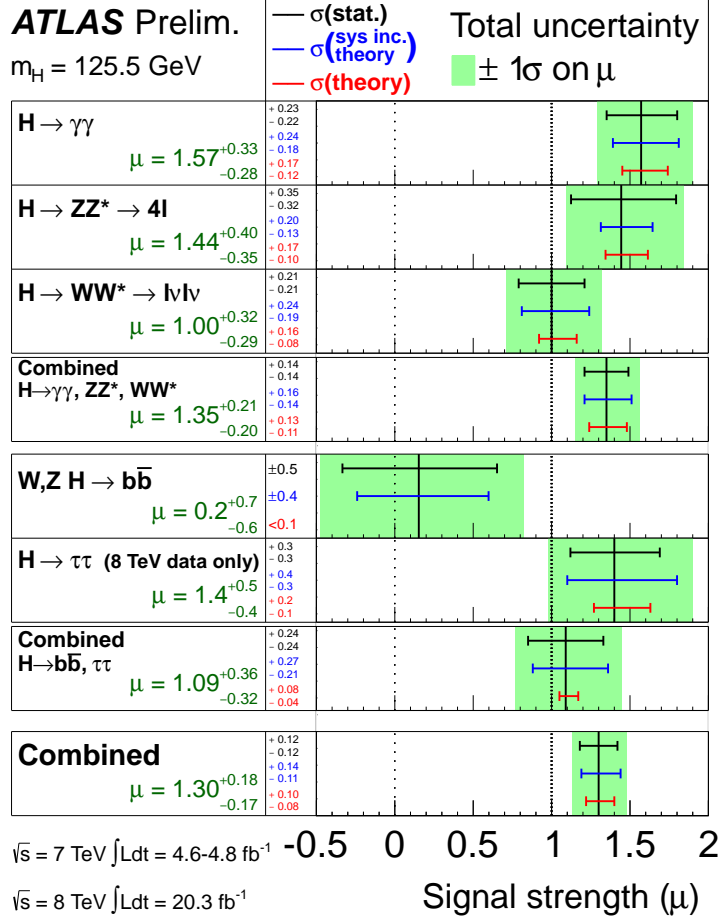
Figure 1: The measured signal strengths for a Higgs boson of mass m_H =125.5 GeV, normalised to the SM expectations, for the individual final states and various combinations. The best-fit values are shown by the solid vertical lines. The total $\pm 1\sigma$ uncertainties are indicated by green shaded bands, with the individual contributions from the statistical uncertainty (top), the total (experimental and theoretical) systematic uncertainty (middle), and the theory uncertainty (bottom) on the signal strength (from QCD scale, PDF, and branching ratios) shown as superimposed error bars. The measurements are based on Refs. [3, 5, 6], with the changes mentioned in the text.

Section 2. In the $H \rightarrow \tau\tau$ channel, the ratio $\mu_{\mathrm{VBF}+VH}/\mu_{\mathrm{ggF}+ttH}$ has an infinite 1σ upper bound, because the signal is almost only observed in the VBF mode, hence the ggF denominator can be arbitrarily small.

To test the sensitivity to VBF production alone, the data are also fitted with the ratio $\mu_{\mathrm{VBF}}/\mu_{\mathrm{ggF}+ttH}$. In order not to influence the VBF measurement through the VH categories, the parameter $\mu_{VH}/\mu_{\mathrm{ggF}+ttH}$ is treated independently and profiled. A value of

$$\mu_{\mathrm{VBF}}/\mu_{\mathrm{ggF}+ttH} = 1.4^{+0.5}_{-0.4}\,(\mathrm{stat})\,^{+0.4}_{-0.3}\,(\mathrm{sys})$$

is obtained from the combination of the four channels (Fig. 4). This result provides evidence at the 4.1σ level that a fraction of Higgs boson production occurs through VBF.

6
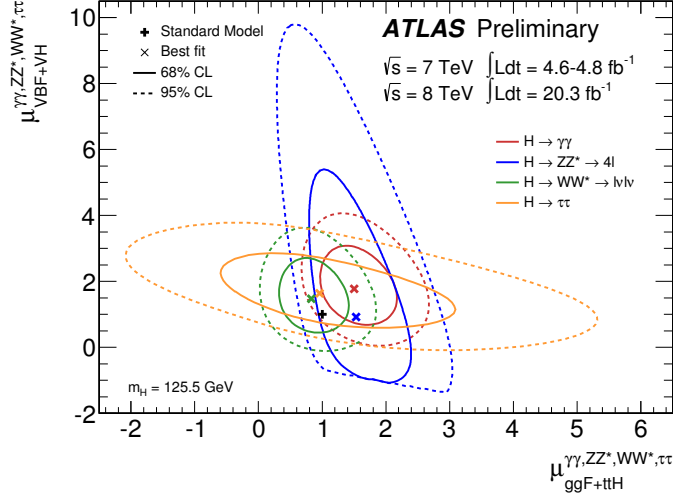
Figure 2: Likelihood contours in the $(\mu_{ggF+ttH}^f, \mu_{VBF+VH}^f)$ plane for the channels $f=H\rightarrow\gamma\gamma$, $H\rightarrow ZZ^*\rightarrow 4\ell$, $H\rightarrow WW^*\rightarrow \ell\nu\ell\nu$, $H\rightarrow\tau\tau$ and a Higgs boson mass $m_H = 125.5$ GeV. The sharp lower edge of the $H\rightarrow ZZ^*\rightarrow 4\ell$ contours is due to the small number of events in this channel and the requirement of a positive pdf. The best-fit values to the data ($\times$) and the 68% (full) and 95% (dashed) CL contours are indicated, as well as the SM expectations (+).

5 Coupling fits

In the previous section signal strength scale factors μ_i^f for given Higgs boson production or decay modes are discussed. However, for a measurement of Higgs boson couplings, production and decay modes cannot be treated independently. Scenarios with a consistent treatment of Higgs boson couplings in production and decay modes are studied in this section. All uncertainties on the best-fit values shown in this Section take into account both experimental and theoretical systematic values.

5.1 Framework for coupling scale factor measurements

Following the leading order (LO) tree level motivated framework and benchmarks recommended in Ref. [14], measurements of coupling scale factors are implemented for the combination of all analyses and channels summarised in Table 1. This framework is based on the following assumptions:

- The signals observed in the different search channels originate from a single narrow resonance with a mass near 125.5 GeV. The case of several, possibly overlapping, resonances in this mass region is not considered.

- The width of the assumed Higgs boson near 125.5 GeV is neglected, i.e. the zero-width approximation is used. Hence the product $\sigma \times BR(i \rightarrow H \rightarrow f)$ can be decomposed in the following way for all channels:

$$\sigma \times BR(i \rightarrow H \rightarrow f) = \frac{\sigma_i \cdot \Gamma_f}{\Gamma_H},$$

where σ_i is the production cross section through the initial state i, Γ_f the partial decay width into the final state f and Γ_H the total width of the Higgs boson.

- Only modifications of couplings strengths, i.e. of absolute values of couplings, are taken into account, while the tensor structure of the couplings is assumed to be the same as in the SM. This
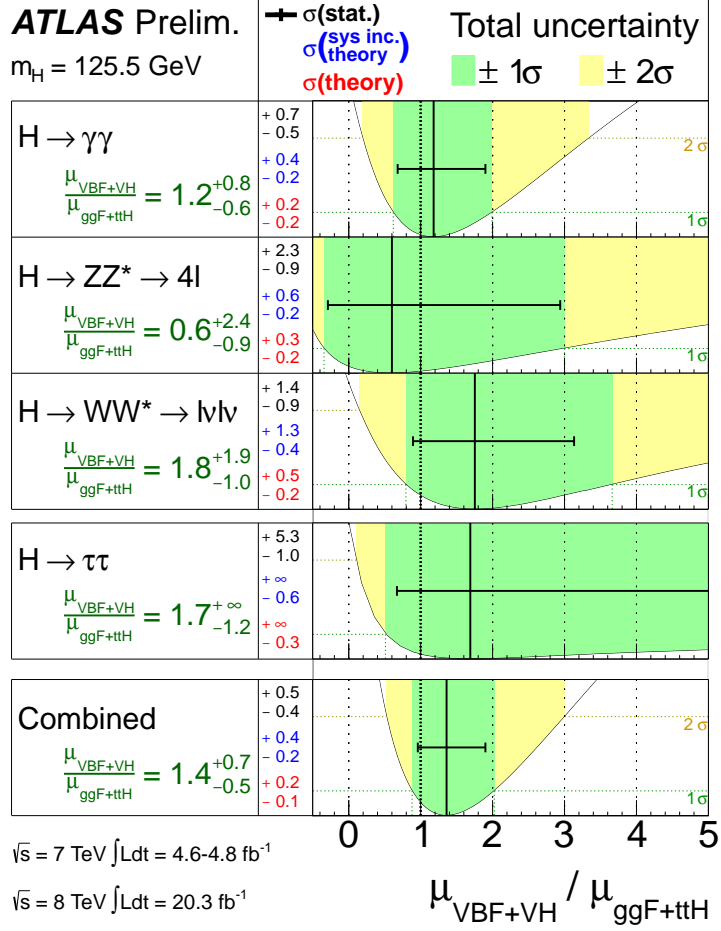
7

Figure 3: Measurements of the $\mu_{VBF+VH}/\mu_{ggF+ttH}$ ratios for the individual final states and their combination, for a Higgs boson mass m_H =125.5 GeV. The best-fit values are represented by the solid vertical lines, with the total $\pm 1\sigma$ and $\pm 2\sigma$ uncertainties indicated by the green and yellow shaded bands, respectively, and the statistical uncertainties by the superimposed horizontal error bars. The numbers in the second column specify the contributions of the statistical uncertainty (top), the total (experimental and theoretical) systematic uncertainty (middle), and the theoretical uncertainty (bottom) on the signal cross section (from QCD scale, PDF, and branching ratios) alone. For a more complete illustration, the likelihood curves from which the total uncertainties are extracted are overlaid. The measurements are based on Refs. [3, 6], with the changes mentioned in the text.

means in particular that the observed state is assumed to be a CP-even scalar as in the SM (this assumption was tested by both the ATLAS [15] and CMS [16] Collaborations).

The LO-motivated coupling scale factors κ_j are defined in such a way that the cross section σ_j and the partial decay width Γ_j associated with the SM particle j scale with the factor κ_j^2 when compared to the corresponding SM prediction. Details can be found in Refs. [14, 17].

In some of the fits the effective scale factors κ_γ and κ_g for the processes $H \to \gamma\gamma$ and $gg \to H$, which are loop-induced in the SM, are treated as a function of the more fundamental coupling scale factors κ_t, κ_b, κ_W, and similarly for all other particles that contribute to these SM loop processes. In these cases the scaled fundamental couplings are propagated through the loop calculations, including all interference effects, using the functional form derived from the SM. Similarly the scaling of the VBF cross section
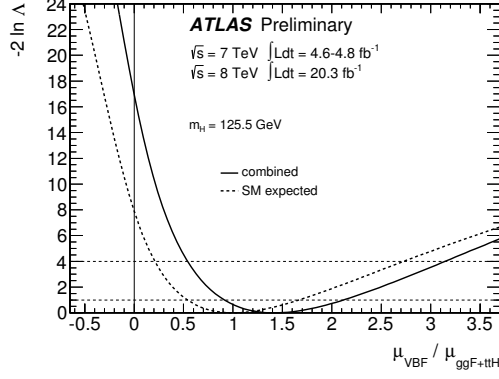
Figure 4: Likelihood curve for the ratio $\mu_{\text{VBF}}/\mu_{\text{ggF}+ttH}$ for the combination of the $H \to \gamma\gamma$, $H \to ZZ^* \to 4\ell$, $H \to WW^* \to \ell\nu\ell\nu$ and $H \to \tau\tau$ channels and a Higgs boson mass $m_H = 125.5$ GeV. The parameter $\mu_{VH}/\mu_{\text{ggF}+ttH}$ is profiled in the fit. The dashed curve shows the SM expectation. The horizontal dashed lines indicate the 68% and 95% CL.

and the total width scale factor κ_H^2 are expressed as functions of the more fundamental coupling scale factors in some fits. To a very good approximation, the relevant expressions for $m_H = 125.5$ GeV are:

$$\kappa_\gamma^2 \sim 1.59 \cdot \kappa_W^2 - 0.66 \cdot \kappa_W \kappa_t + 0.07 \cdot \kappa_t^2 \tag{2}$$

$$\kappa_g^2 \sim 1.06 \cdot \kappa_t^2 - 0.07 \cdot \kappa_t \kappa_b + 0.01 \cdot \kappa_b^2 \tag{3}$$

$$\kappa_{\text{VBF}}^2 \sim 0.74 \cdot \kappa_W^2 + 0.26 \cdot \kappa_Z^2 \tag{4}$$

$$\kappa_H^2 \sim 0.57 \cdot \kappa_b^2 + 0.22 \cdot \kappa_W^2 + 0.09 \cdot \kappa_g^2 + 0.06 \cdot \kappa_\tau^2 + 0.03 \cdot \kappa_Z^2 + 0.03 \cdot \kappa_c^2. \tag{5}$$

For details and the exact expressions used, see Appendix A and Ref. [14].

The assumptions made for the various measurements are summarised in Table 2 and discussed in the next sections together with the results. The functional dependence of the signal strengths on the effective scale factors κ_j is explicated for each benchmark model considered and for the most important Higgs boson production and decay modes in Appendix A.

5.2 Fermion versus vector (gauge) couplings

This benchmark is an extension of the fit to the single parameter μ, where different strengths for the fermion and vector couplings are probed. It assumes that only SM particles contribute to the $H \to \gamma\gamma$ and $gg \to H$ vertex loops, and modifications of the coupling strength factors for fermions and vector bosons are propagated through the loop calculations. The fit is performed in two variants, with and without the assumption that the total width of the Higgs boson is given by the sum of the known SM Higgs boson decay modes (modified in strength by the appropriate fermion and vector coupling scale factors).

5.2.1 Only SM contributions to the total width

The fit parameters are the coupling scale factors κ_F for all fermions and κ_V for all vector couplings:

$$\kappa_V = \kappa_W = \kappa_Z$$
$$\kappa_F = \kappa_t = \kappa_b = \kappa_\tau = \kappa_g.$$

As only SM particles are assumed to contribute to the $gg \to H$ vertex loop in this benchmark, the gluon fusion process depends directly on the fermion scale factor κ_F^2. The relevant scaling formulae can be found in Appendix A.1.1.

9

Table 2: Summary of the coupling benchmark models discussed in this note, where $\lambda_{ij} = \kappa_i/\kappa_j$, $\kappa_{ii} = \kappa_i\kappa_i/\kappa_H$, and the functional dependence assumptions are: $\kappa_V = \kappa_W = \kappa_Z$, $\kappa_F = \kappa_t = \kappa_b = \kappa_\tau$ (and similarly for the other fermions), $\kappa_g = \kappa_g(\kappa_b, \kappa_t)$, $\kappa_\gamma = \kappa_\gamma(\kappa_b, \kappa_t, \kappa_\tau, \kappa_W)$, and $\kappa_H = \kappa_H(\kappa_i)$. The tick marks indicate which assumptions are made in each case. The last column shows, as an example, the relative couplings involved in the $gg \to H \to \gamma\gamma$ process (see Appendix A for more details).

Section	Probed couplings	Parameters of interest	κ_V	κ_F	κ_g	κ_γ	κ_H	Example: $gg \to H \to \gamma\gamma$
5.2.1	Couplings to fermions and bosons	κ_V, κ_F	√	√	√	√	√	$\kappa_F^2 \cdot \kappa_\gamma^2(\kappa_F, \kappa_V)/\kappa_H^2(\kappa_F, \kappa_V)$
5.2.2		$\lambda_{FV}, \kappa_{VV}$	√	√	√	√	-	$\kappa_{VV}^2 \cdot \lambda_{FV}^2 \cdot \kappa_\gamma^2(\lambda_{FV}, \lambda_{FV}, \lambda_{FV}, 1)$
5.3	Custodial symmetry	$\lambda_{WZ}, \lambda_{FZ}, \kappa_{ZZ}$	-	√	√	√	-	$\kappa_{ZZ}^2 \cdot \lambda_{FZ}^2 \cdot \kappa_\gamma^2(\lambda_{FZ}, \lambda_{FZ}, \lambda_{FZ}, \lambda_{WZ})$
5.4.1	Up-/down-type fermions	$\lambda_{du}, \lambda_{Vu}, \kappa_{uu}$	√	κ_u, κ_d	√	√	-	$\kappa_{uu}^2 \cdot \kappa_g^2(\lambda_{du}, 1) \cdot \kappa_\gamma^2(\lambda_{du}, 1, \lambda_{du}, \lambda_{Vu})$
5.4.2	Leptons/Quarks	$\lambda_{lq}, \lambda_{Vq}, \kappa_{qq}$	√	κ_l, κ_q	√	√	-	$\kappa_{qq}^2 \cdot \kappa_\gamma^2(1, 1, \lambda_{lq}, \lambda_{Vq})$
5.5.1	Vertex loops	κ_g, κ_γ	=1	=1	-	-	√	$\kappa_g^2 \cdot \kappa_\gamma^2/\kappa_H^2(\kappa_g, \kappa_\gamma)$
5.5.2	+ H→inv./undet. decays	$\kappa_g, \kappa_\gamma, \mathrm{BR}_{i.,u.}$	=1	=1	-	-	√	$\kappa_g^2 \cdot \kappa_\gamma^2/\kappa_H^2(\kappa_g, \kappa_\gamma) \cdot (1 - \mathrm{BR}_{i.,u.})$
5.6.1	Generic models with and without assumptions on vertex loops and Γ_H	$\kappa_W, \kappa_Z, \kappa_t, \kappa_b, \kappa_\tau$	-	-	√	√	√	$\dfrac{\kappa_g^2(\kappa_b,\kappa_t) \cdot \kappa_\gamma^2(\kappa_b,\kappa_t,\kappa_\tau,\kappa_W)}{\kappa_H^2(\kappa_b,\kappa_t,\kappa_\tau,\kappa_W,\kappa_Z)}$
5.6.2		$\lambda_{WZ}, \lambda_{tg}, \lambda_{bZ}, \lambda_{\tau Z},$ $\lambda_{gZ}, \lambda_{\gamma Z}, \kappa_{gZ}$	-	-	-	-	-	$\kappa_{gZ}^2 \cdot \lambda_{\gamma Z}^2$

Figure 5 shows the results for this benchmark. Only the relative sign between κ_F and κ_V is physical and hence in the following only $\kappa_V > 0$ is considered, without loss of generality. Sensitivity to this relative sign is gained from the negative interference between the loop contributions of the W boson and the t quark in the $H \to \gamma\gamma$ decay (see Eq. 2). As can be seen in Fig. 5(a) the fit prefers the SM-like minimum with a positive relative sign, while the local minimum with negative relative sign is disfavoured at the $\sim 2\sigma$ level. Figure 5(b) illustrates how the $H \to \gamma\gamma$, $H \to ZZ^*$, $H \to WW^*$, $H \to \tau\tau$ and $H \to b\bar{b}$ channels contribute to the combined measurement. The likelihoods are given in Figs. 5(c) and 5(d), as a function of κ_V when κ_F is profiled, and as a function of κ_F when κ_V is profiled. Figure 5(d) shows in particular to what extent the sign degeneracy is resolved.

The best-fit values and uncertainties, when the other parameter is profiled, are:

$$\kappa_V = 1.15 \pm 0.08$$
$$\kappa_F = 0.99^{+0.17}_{-0.15}.$$

The two-dimensional compatibility of the SM hypothesis with the best-fit point is 10%. With respect to the diboson final state combination in Ref. [3], by coincidence the central value is almost unchanged, while the uncertainty on κ_F is reduced substantially.

5.2.2 No assumption on the total width

The assumption on the total width gives a strong constraint on the fermion coupling scale factor κ_F in the previous benchmark model, as the total width is dominated in the SM by the sum of the fermion-induced b, τ and gluon-decay widths. The fit is therefore repeated without the assumption on the total width.

In this case only ratios of coupling scale factors can be measured. Hence there are the following free parameters:

$$\lambda_{FV} = \kappa_F/\kappa_V$$
$$\kappa_{VV} = \kappa_V \cdot \kappa_V/\kappa_H,$$

where λ_{FV} is the ratio of the fermion and vector boson coupling scale factors, and κ_{VV} an overall scale that includes the total width and applies to all rates. The relevant scaling formulae can be found in Appendix A.1.2.
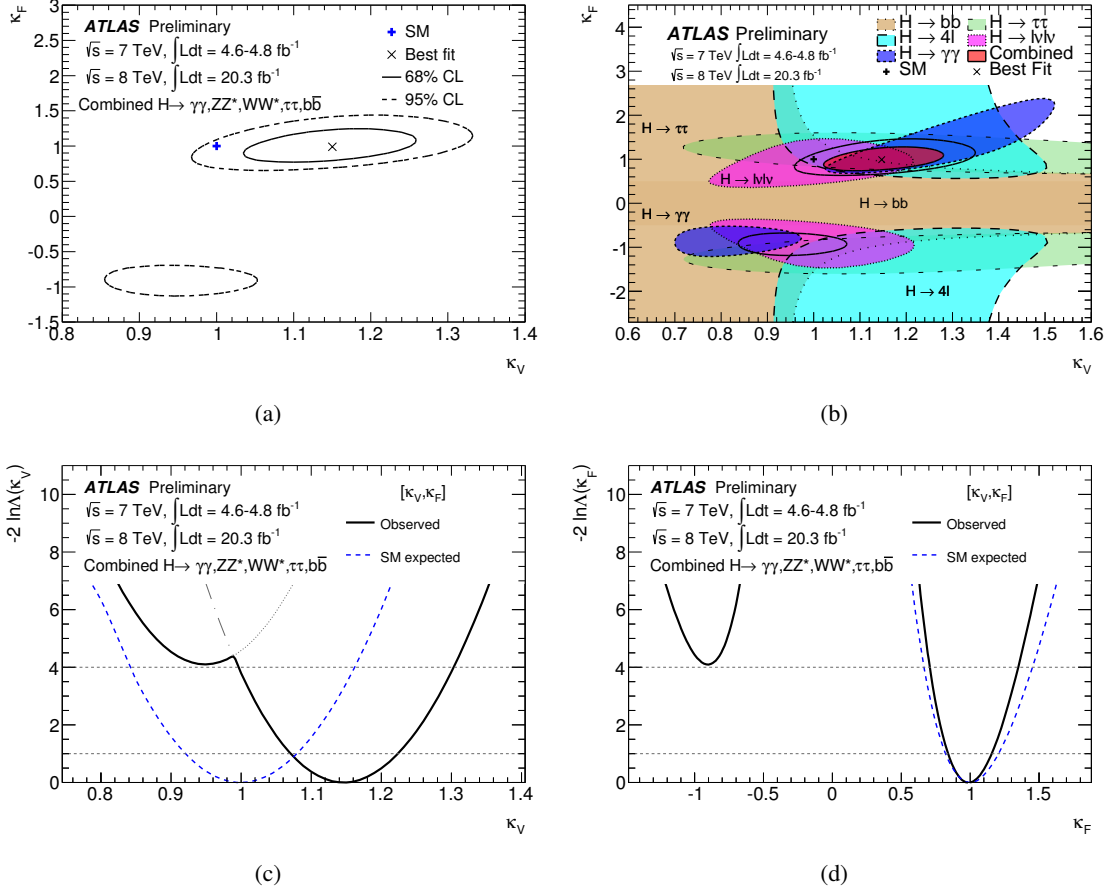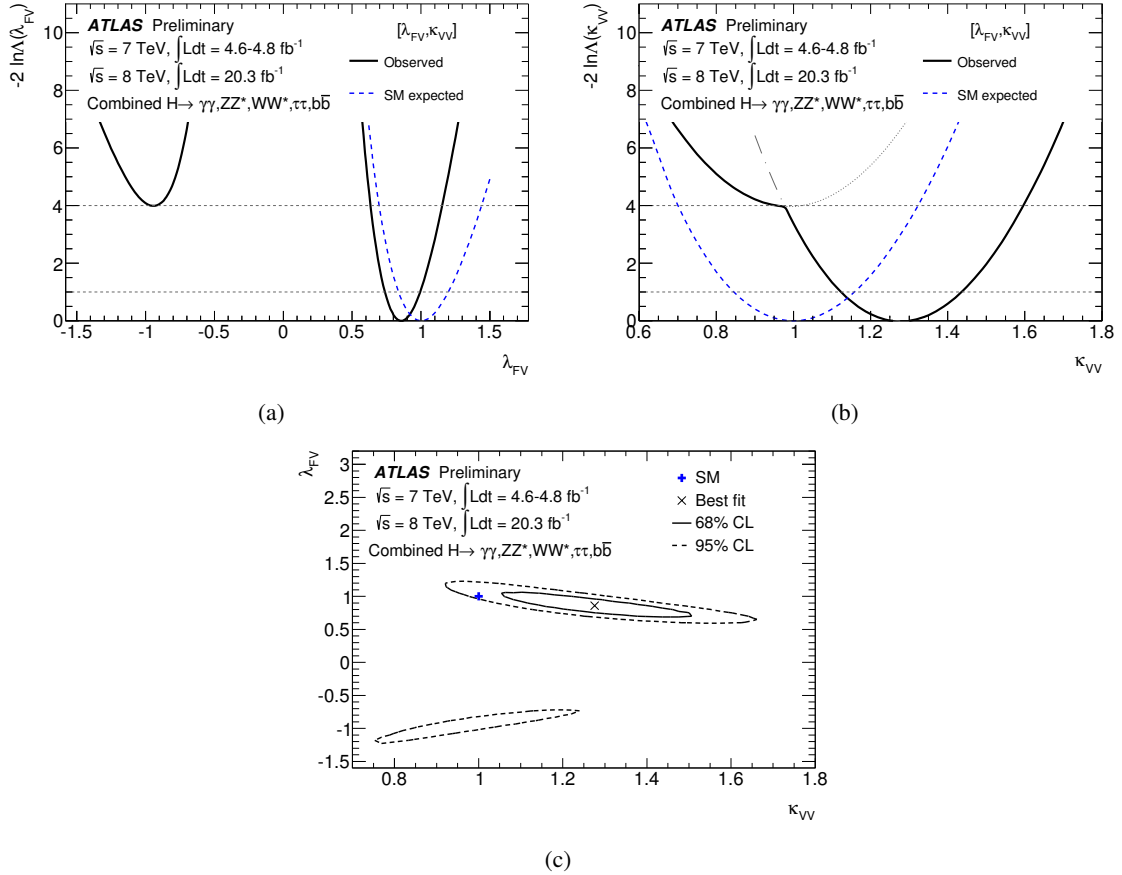
Figure 5: Results of fits for the 2-parameter benchmark model defined in Section 5.2.1 that probe different coupling strength scale factors for fermions and vector bosons, assuming only SM contributions to the total width: (a) Correlation of the coupling scale factors κ_F and κ_V; (b) the same correlation, overlaying the 68% CL contours derived from the individual channels and their combination; (c) coupling scale factor κ_V (κ_F is profiled); (d) coupling scale factor κ_F (κ_V is profiled). The dashed curves in (c) and (d) show the SM expectations. The thin dotted and dash-dotted lines in (c) indicate the continuations of the likelihood curves when restricting the parameters to either the positive or negative sector of κ_F.

Figure 6 shows the results of this fit. The best-fit values and uncertainties, when profiling the other parameter, are:

$$\lambda_{FV} = 0.86^{+0.14}_{-0.12}$$
$$\kappa_{VV} = 1.28^{+0.16}_{-0.15}.$$

Similarly to the above case, Figure 6(a) shows the determination of the sign of λ_{FV}. Figure 6(c) shows the two-dimensional likelihood contours. The two variables are anticorrelated because only their product appears in the model. The two-dimensional compatibility of the SM hypothesis with the best-fit point is 10%.

(a)

(b)

(c)

Figure 6: Results of fits for the 2-parameter benchmark model defined in Section 5.2.2 that probe different coupling strength scale factors for fermions and vector bosons without assumptions on the total width: (a) coupling scale factor ratio λ_{FV} (κ_{VV} is profiled); (b) coupling scale factor ratio κ_{VV} (λ_{FV} is profiled). The dashed curves show the SM expectations. The thin dotted and dashed-dotted lines in (b) indicate the continuations of the likelihood curves when restricting the parameters to either the positive or negative sector of λ_{FV}; (c) correlation contours of the same variables.

5.2.3 Summary

The coupling of the new particle to fermions is observed directly in the $H \rightarrow \tau\tau$ channel at more than 4σ [6], while the $H \rightarrow b\bar{b}$ channel is compatible both with the SM Higgs boson and SM background. This coupling is also observed indirectly through the constraints from the channels which are dominated

by the main production process $gg \rightarrow H$, assumed to be fermion-mediated in this benchmark model. The relatively large values of κ_V in the first model and κ_{VV} in the second model reflect the large μ values measured for the bosonic modes.

5.3 Probing the custodial symmetry of the W and Z couplings

Identical coupling scale factors for the W and Z boson are required within tight bounds by the SU(2) custodial symmetry and the ρ parameter measurements at LEP and at the Tevatron [18]. To test this constraint directly in the Higgs sector, the ratio $\lambda_{WZ} = \kappa_W/\kappa_Z$ is probed. For the other parameters the same assumptions as in Section 5.2.1 on κ_F are made ($\kappa_F = \kappa_t = \kappa_b = \kappa_\tau$). The free parameters are:

$$\begin{aligned}
\lambda_{WZ} &= \kappa_W/\kappa_Z \\
\lambda_{FZ} &= \kappa_F/\kappa_Z \\
\kappa_{ZZ} &= \kappa_Z \cdot \kappa_Z/\kappa_H.
\end{aligned}$$

The relevant scaling formulae can be found in Appendix A.2.

The ratio λ_{WZ} is in part directly constrained by the decays in the $H \rightarrow WW^* \rightarrow \ell\nu\ell\nu$ and $H \rightarrow ZZ^* \rightarrow 4\ell$ channels and the WH and ZH production processes. It is also indirectly constrained by the VBF production process, which in the SM is 74% W fusion and 26% Z fusion-mediated (see Eq. 4). The scale factor κ_W is also constrained by the $H \rightarrow \gamma\gamma$ channel since the decay branching ratio receives a dominant contribution from the W loop.

Figure 7 shows the likelihood functions for this benchmark scenario. There is a relative sign ambiguity between the W and Z boson couplings. However, this relative sign is not accessible at the LHC[6]. The sign of λ_{WZ} can be chosen positive without loss of generality.

The fit prefers the SM-like local minimum with a positive sign for λ_{FZ}, implying a positive relative sign between the fermion and Z couplings, while the negative sign is still compatible at the $\sim 1\sigma$ level. The minimum corresponding to negative λ_{FZ} values is seen in Fig. 7(a) as the left branch of the observed and expected curves, and in Fig. 7(b).

The fit results for the parameters of interest, when profiling the other parameters, are:

$$\begin{aligned}
\lambda_{WZ} &= 0.94^{+0.14}_{-0.29} \\
\lambda_{FZ} &\in [-0.91, -0.63] \cup [0.65, 1.00] \\
\kappa_{ZZ} &= 1.41^{+0.49}_{-0.34}.
\end{aligned}$$

The three-dimensional compatibility of the SM hypothesis with the best-fit point is 19%. In the diboson final state combination of Ref. [3], the minimum at negative λ_{FZ} was disfavoured for the expectation, but the minima of the two branches were found to be similar for the data, due to the high value of the signal strength in the $H \rightarrow \gamma\gamma$ channel. With the addition of the direct fermion decay channels, the non-SM-like minimum is now also slightly disfavoured in the data.

In order to be independent of possible new physics contributions to the $H \rightarrow \gamma\gamma$ channel, the same analysis can be performed with an effective coupling scale factor ratio $\lambda_{\gamma Z}$ which is profiled in the measurement of λ_{WZ} (see Ref. [3]). The measured value of λ_{WZ} is in agreement with the expectation of custodial symmetry $\lambda_{WZ} = 1$, regardless of the inclusion of the $H \rightarrow \gamma\gamma$ channel as an indirect constraint on κ_W. With the availability of the direct fermion channels, this case is now covered by the generic model in Section 5.6.2, which yields consistent results.

---

[6]In principle the VBF process has some sensitivity to the W and Z interference, but the interference term is $\ll 1\%$ and hence too small to have any discriminating power.
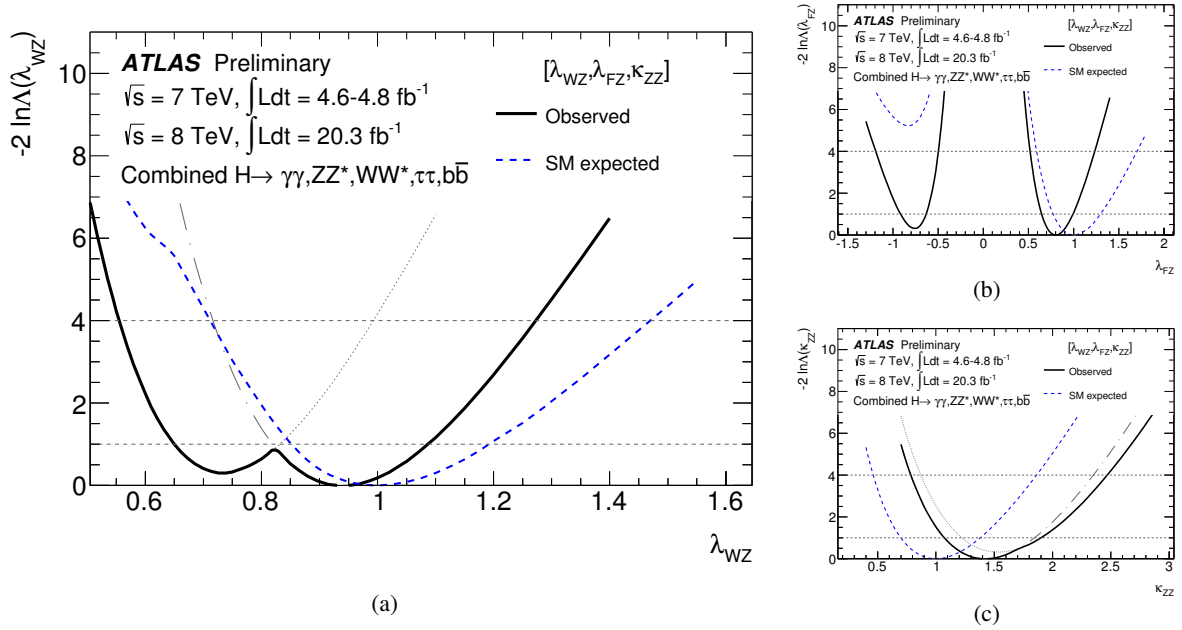
Figure 7: Results of fits for the benchmark model defined in Section 5.3 that probe the custodial symmetry through the ratio $\lambda_{WZ} = \kappa_W/\kappa_Z$: (a) coupling scale factor ratio λ_{WZ} (λ_{FZ} and κ_{ZZ} are profiled); (b) coupling scale factor ratio λ_{FZ} (λ_{WZ} and κ_{ZZ} are profiled); (c) overall scale factor κ_{ZZ} (λ_{WZ} and λ_{FZ} are profiled). The dashed curves show the SM expectations. The thin dotted/dashed-dotted lines indicate the continuations of the likelihood curves when restricting the parameters to either the positive or negative sector of λ_{FZ}.

5.4 Probing relations within the fermion coupling sector

The previous sections assumed universal coupling scale factors for all fermions, while many extensions of the SM predict deviations within the fermion sector. The currently accessible channels, in particular with the addition of $H \to b\bar{b}$ and $H \to \tau\tau$, allow the relations between the up- and down-type fermion sector and between the lepton and quark sector to be probed.

5.4.1 Probing the up- and down-type fermion symmetry

Many extensions of the SM contain different couplings of the Higgs boson to up-type and down-type fermions. This is for instance the case for certain Two-Higgs-Doublet Models [14, 19–21], among which the MSSM is the most prominent example. In this model the ratio λ_{du} between down- and up-type fermions is probed, while vector boson couplings are taken unified as κ_V. The indices u, d stand for all up- and down-type fermions, respectively. The free parameters are:

$$\lambda_{du} = \kappa_d/\kappa_u$$
$$\lambda_{Vu} = \kappa_V/\kappa_u$$
$$\kappa_{uu} = \kappa_u \cdot \kappa_u/\kappa_H.$$

The relevant scaling formulae can be found in Appendix A.3.1.

The up-type quark coupling scale factor is mostly indirectly constrained through the $gg \to H$ production channel, from the Higgs boson to top-quark coupling, while the down-type coupling strength is constrained through the $H \to b\bar{b}$ and $H \to \tau\tau$ decays. Figure 8 shows the results for this benchmark scenario. The likelihood curve is nearly symmetric about $\lambda_{du} = 0$ as the model is almost insensitive to

14

the relative sign of κ_u and κ_d. The interference of contributions from the b and t loops in the $gg \to H$ production induces an asymmetry, much smaller than the present sensitivity (see Eq. 3). The fit results for the parameters of interest are:

$$
\begin{aligned}
\lambda_{du} &\in [-1.24, -0.81] \cup [0.78, 1.15] \\
\lambda_{Vu} &= 1.21^{+0.24}_{-0.26} \\
\kappa_{uu} &= 0.86^{+0.41}_{-0.21}.
\end{aligned}
$$

The value of λ_{du} around the SM-like minimum at 1 is $\lambda_{du} = 0.95^{+0.20}_{-0.18}$. This fit provides a $\sim 3.6\sigma$ level evidence of the coupling of the Higgs boson to down-type fermions, mostly coming from the $H \to \tau\tau$ measurement. The three-dimensional compatibility of the SM hypothesis with the best-fit point is 20%.
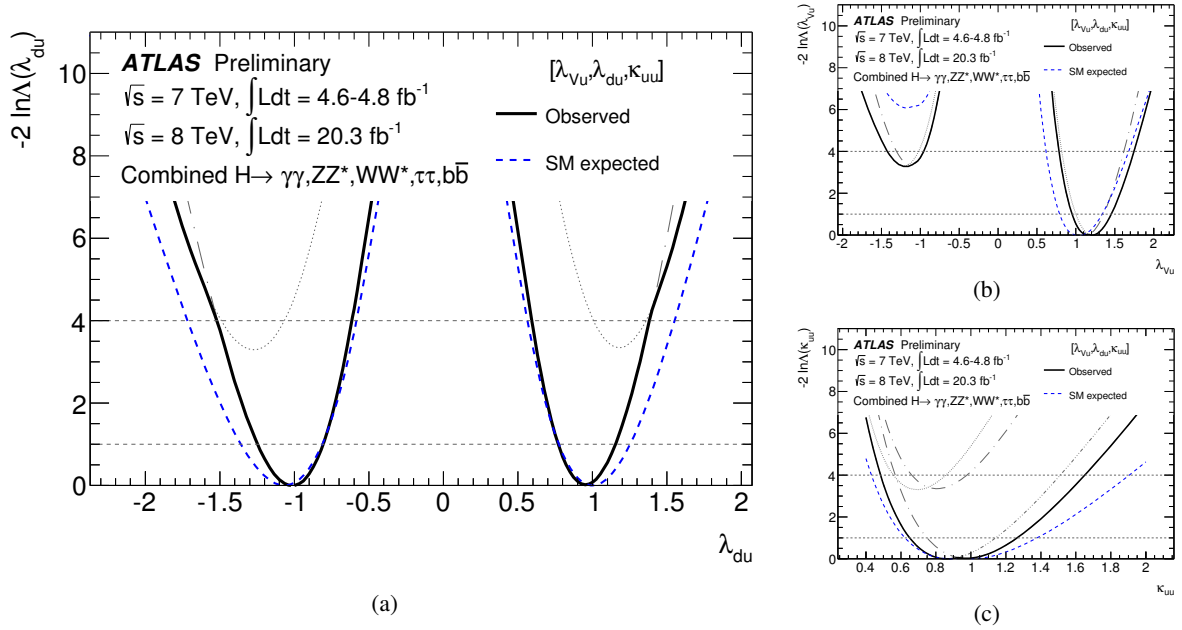
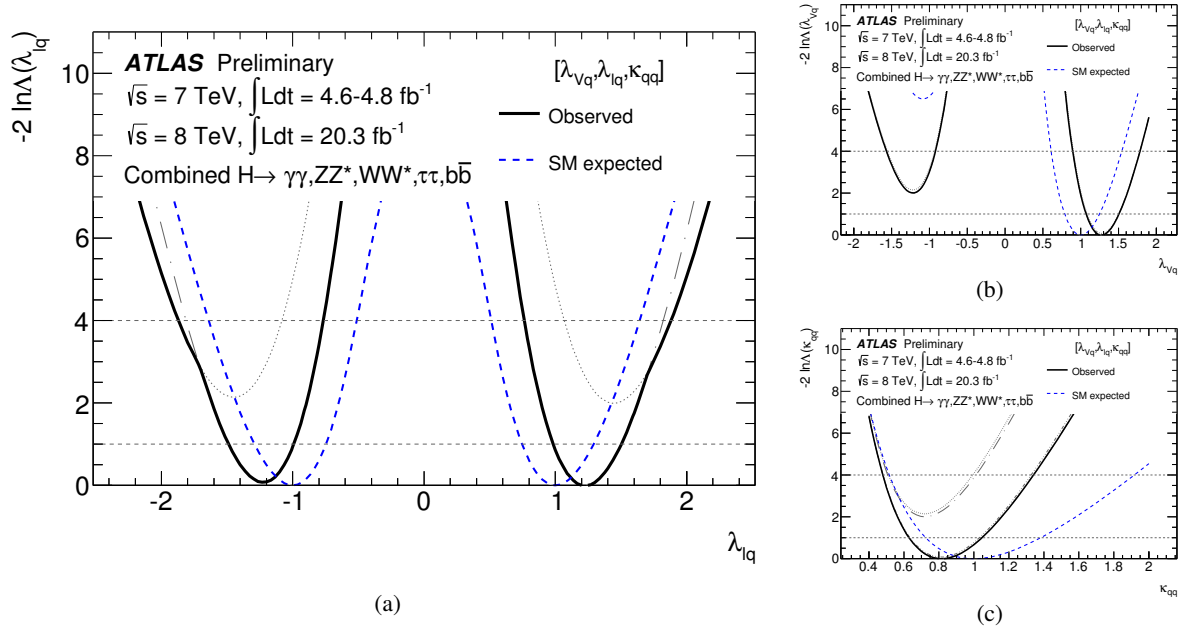Figure 8: Results of fits for the benchmark model described in Section 5.4.1 that probe the symmetry between down- and up-type fermions: (a) coupling scale factor ratio λ_{du} (λ_{Vu} and κ_{uu} are profiled); (b) coupling scale factor ratio λ_{Vu} (λ_{du} and κ_{uu} are profiled); (c) overall scale factor κ_{uu} (λ_{du} and λ_{Vu} are profiled). The dashed curves show the SM expectations. The thin dotted/dashed-dotted lines indicate the continuations of the likelihood curves when restricting the parameters to either the positive or negative sector of λ_{du} and λ_{Vu}, respectively.

5.4.2 Probing the quark and lepton symmetry

Here the ratio λ_{lq} between leptons and quarks is probed, while vector boson couplings are taken unified as κ_V. The indices l, q stand for all leptons and quarks, respectively. The free parameters are:

$$
\begin{aligned}
\lambda_{lq} &= \kappa_l/\kappa_q \\
\lambda_{Vq} &= \kappa_V/\kappa_q \\
\kappa_{qq} &= \kappa_q \cdot \kappa_q/\kappa_H.
\end{aligned}
$$

The relevant scaling formulae can be found in Appendix A.3.2. The lepton coupling strength is currently only constrained through the $H \to \tau\tau$ decay.

Figure 9 shows the results for this benchmark. Similar to the case above, the likelihood curve is nearly symmetric about $\lambda_{lq} = 0$. The fit results for the parameters of interest are:

$$\begin{aligned}
\lambda_{lq} &\in& [-1.48, -0.99] \cup [0.99, 1.50] \\
\lambda_{Vq} &=& 1.27^{+0.23}_{-0.20} \\
\kappa_{qq} &=& 0.82^{+0.23}_{-0.19}.
\end{aligned}$$

The value of λ_{lq} around the SM-like minimum at 1 is $\lambda_{lq} = 1.22^{+0.28}_{-0.24}$. A vanishing coupling of the Higgs boson to leptons is excluded at the $\sim 4.0\sigma$ level due to the $H \to \tau\tau$ measurement. The three-dimensional compatibility of the SM hypothesis with the best-fit point is 15%.

(a)

(b)

(c)

Figure 9: Results of fits for the benchmark model described in Section 5.4.2 that probe the symmetry between quarks and leptons: (a) coupling scale factor ratio λ_{lq} (λ_{Vq} and κ_{qq} are profiled); (b) coupling scale factor ratio λ_{Vq} (λ_{lq} and κ_{qq} are profiled); (c) overall scale factor κ_{qq} (λ_{lq} and λ_{Vq} are profiled). The dashed curves show the SM expectations. The thin dotted/dashed-dotted lines indicate the continuations of the likelihood curves when restricting the parameters to either the positive or negative sector of λ_{lq} and λ_{Vq}, respectively.

5.5 Probing beyond the SM contributions

In this section contributions from new particles either in loops or in new final states are considered. All coupling scale factors of known SM particles are assumed to be as predicted by the SM, i.e. $\kappa_i = 1$. For the $H \to \gamma\gamma$ and $gg \to H$ vertices, effective scale factors κ_γ and κ_g are introduced that allow for extra contributions from new particles. The potential new particles contributing to the $H \to \gamma\gamma$ and $gg \to H$ loops may or may not contribute to the total width of the observed state through direct invisible decays or decays into final states that cannot be distinguished from the background. In these cases the resulting variation in the total width is parameterised in terms of the additional branching ratio into invisible or undetected particles $BR_{i.,u.}$ [7]. Both aforementioned scenarios are addressed in this section.

---

[7]Invisible final states can be directly searched for through the E_T^{miss} signature [22]. An example of an undetected mode would be a decay mode to multiple light jets, which presently cannot be distinguished from multi-jet backgrounds.

16

5.5.1 Only SM contributions to the total width

In the first benchmark model it is assumed that there are no sizeable extra contributions to the total width caused by non-SM particles. The free parameters are κ_g and κ_γ. The relevant scaling formulae can be found in Appendix A.4.1.

Figure 10 shows the results of fits for this benchmark scenario. The best-fit values and uncertainties, when profiling the other parameter, are:

$$\kappa_g = 1.08^{+0.15}_{-0.13}$$
$$\kappa_\gamma = 1.19^{+0.15}_{-0.12}.$$

The two-dimensional compatibility of the SM hypothesis with the best-fit point is 9%. With respect to the results from the combination of the diboson final states in Ref. [3], the contours for κ_g and κ_γ are almost unchanged, as the direct fermion decay channels have only a minor impact on these degrees of freedom.

5.5.2 No assumption on the total width

By constraining some of the factors to be equal to their SM values, it is possible to probe for new non-SM decay modes with a branching ratio $BR_{i.,u.}$ that might yield invisible or undetected final states. The free parameters in this case are κ_g, κ_γ and $BR_{i.,u.}$. In this model the modification to the total width is parametrised as follows:

$$\Gamma_H = \frac{\kappa_H^2(\kappa_i)}{(1 - BR_{i.,u.})}\Gamma_H^{SM}.$$

The relevant scaling formulae can be found in Appendix A.4.2.

Figure 11 shows the results of fits from this benchmark scenario. The best-fit values and their uncertainties, when profiling the other parameters, are:

$$\kappa_g = 1.00^{+0.23}_{-0.16}$$
$$\kappa_\gamma = 1.17^{+0.16}_{-0.13}$$

and

$$BR_{i.,u.} = -0.16^{+0.29}_{-0.30}.$$

The three-dimensional compatibility of the SM hypothesis with the best-fit point is 18%. Using the physical constraint $BR_{i.,u.} > 0$ the 95% CL upper limit is $BR_{i.,u.} < 0.41$ (the SM expected limit is $BR_{i.,u.} < 0.55$). The 95% confidence interval is based on the profile likelihood ratio restricted to the allowed region of parameter space; however, the confidence interval is defined by the standard χ^2 cutoff, which leads to some overcoverage near the boundaries.

As the choice of free parameters in this model gives extra degrees of freedom to the $gg \to H$ production and the $H \to \gamma\gamma$ decay, the most precise measurements in Fig. 1 do not give a sizeable contribution to the determination of $BR_{i.,u.}$. Instead $BR_{i.,u.}$ is mostly constrained from channels sensitive to VBF and VH production, as the tree level couplings involved in these production modes are fixed to their SM values within this model. Hence the updated results for the $H \to b\bar{b}$ and $H \to \tau\tau$ channels give a significant improvement in the determination of $BR_{i.,u.}$ compared to the results presented in Ref. [17].
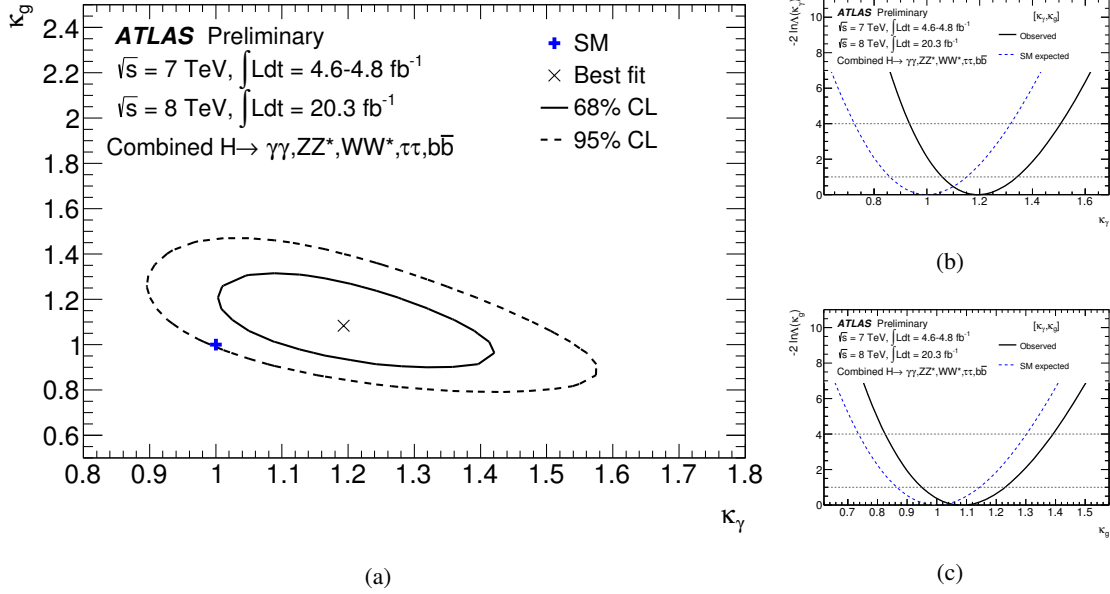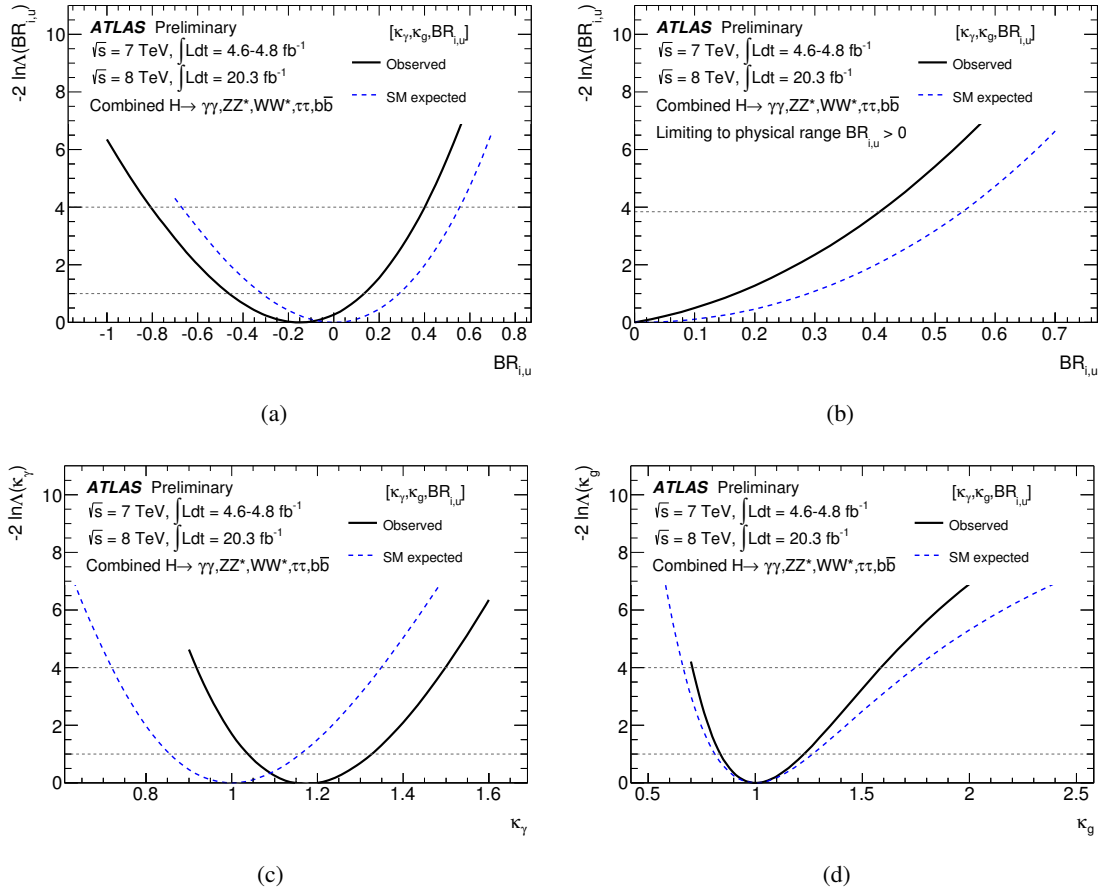
Figure 10: Results of fits for the benchmark models that probe for contributions from non-SM particles in the $H \to \gamma\gamma$ and $gg \to H$ loops, assuming no sizeable extra contributions to the total width: (a) correlation of the coupling scale factors κ_γ and κ_g; (b) coupling scale factor κ_γ (κ_g is profiled); (c) coupling scale factor κ_g (κ_γ is profiled). The dashed curves in (b) and (c) show the SM expectations.

Figure 11: Results of fits for benchmark models that probe for contributions from non-SM particles in the $H \to \gamma\gamma$ and $gg \to H$ loops, while allowing for potential extra contributions to the total width: (a) branching fraction $BR_{i,u}$ to invisible or undetected decay modes (κ_γ and κ_g are profiled); (b) same as (a), but restricting to $BR_{i,u} > 0$ for the extraction of the upper 95% CL limit; (c) coupling scale factor κ_γ (κ_g and $BR_{i,u}$ are profiled); (d) coupling scale factor κ_g (κ_γ and $BR_{i,u}$ are profiled). The dashed curves show the SM expectations.

18

5.5.3 Summary

Under the hypothesis that all tree level couplings of the new boson to SM particles are fixed to their SM values, no significant deviations are observed in the effective couplings to photons and gluons (κ_γ and κ_g, respectively) regardless of the assumption on the total width. Releasing the assumption on the total width constrains $BR_{i.,u.}$ to < 0.41 at 95% CL.

5.6 Generic models

In the previous benchmark models specific aspects of the Higgs sector were tested by combining coupling scale factors into a minimum number of parameters that are sensitive to the probed scenario. Within the following generic models the couplings scale factors to W, Z, t, b and τ are treated independently, while for the $gg \rightarrow H$ production, $H \rightarrow \gamma\gamma$ decay and the total width Γ_H either the SM particle content is assumed or no assumptions are made.

5.6.1 Generic model 1: only SM particles in loops and total width fixed to the SM value

In this benchmark scenario, all couplings to SM particles, relevant to the measured modes, are fitted independently. The free parameters are: κ_W, κ_Z, κ_b, κ_τ, κ_t, while the vertex loop factors and the total width are calculated as a function of these parameters (see Appendix A, Eqs. 6-9). Without loss of generality the W and Z coupling scale factors are assumed to be positive. The relevant scaling formulae can be found in Appendix A.5.1. Due to the interference terms in $gg \rightarrow H$ and $H \rightarrow \gamma\gamma$, Eqs. 2-3, the fit is mainly sensitive to the relative sign between the W- and top-coupling ($H \rightarrow \gamma\gamma$) and also slightly to the relative sign between the top- and bottom-coupling ($gg \rightarrow H$). In principle $H \rightarrow \gamma\gamma$ is also sensitive to the relative sign between W and τ, but the effect is far too small to be observable. Figure 12 shows the results of the fits for this benchmark scenario. The five-dimensional compatibility of the SM hypothesis with the best-fit point is 13%. In Fig. 12(c), the negative minimum of κ_t is expected to be disfavoured, but it is found to be comparable with the positive one, again due to the high signal strength in the $H \rightarrow \gamma\gamma$ mode. The corresponding fitted values of the relative couplings can be found in Fig. 14(a).

5.6.2 Generic Model 2: allowing deviations in vertex loop couplings and the total width

In this case the five free parameters from model 1 are retained but here the assumptions about which particles contribute to the loops and the total width are dropped. Effective coupling scale factors for the $gg \rightarrow H$ and $H \rightarrow \gamma\gamma$ vertices are introduced, resulting in a total of 7 free parameters. As before, without the assumption on the total width, only ratios of coupling scale factors can be measured. The free parameters are:

$$
\begin{aligned}
\lambda_{\gamma Z} &= \kappa_\gamma / \kappa_Z \\
\lambda_{WZ} &= \kappa_W / \kappa_Z \\
\lambda_{bZ} &= \kappa_b / \kappa_Z \\
\lambda_{\tau Z} &= \kappa_\tau / \kappa_Z \\
\lambda_{gZ} &= \kappa_g / \kappa_Z \\
\lambda_{tg} &= \kappa_t / \kappa_g \\
\kappa_{gZ} &= \kappa_g \cdot \kappa_Z / \kappa_H.
\end{aligned}
$$

The relevant scaling formulae can be found in Appendix A.5.2.

Figure 13 shows the results for this benchmark. As the loop-induced processes are expressed by effective coupling scale factors, there is no sensitivity to the relative sign between coupling scale factors.
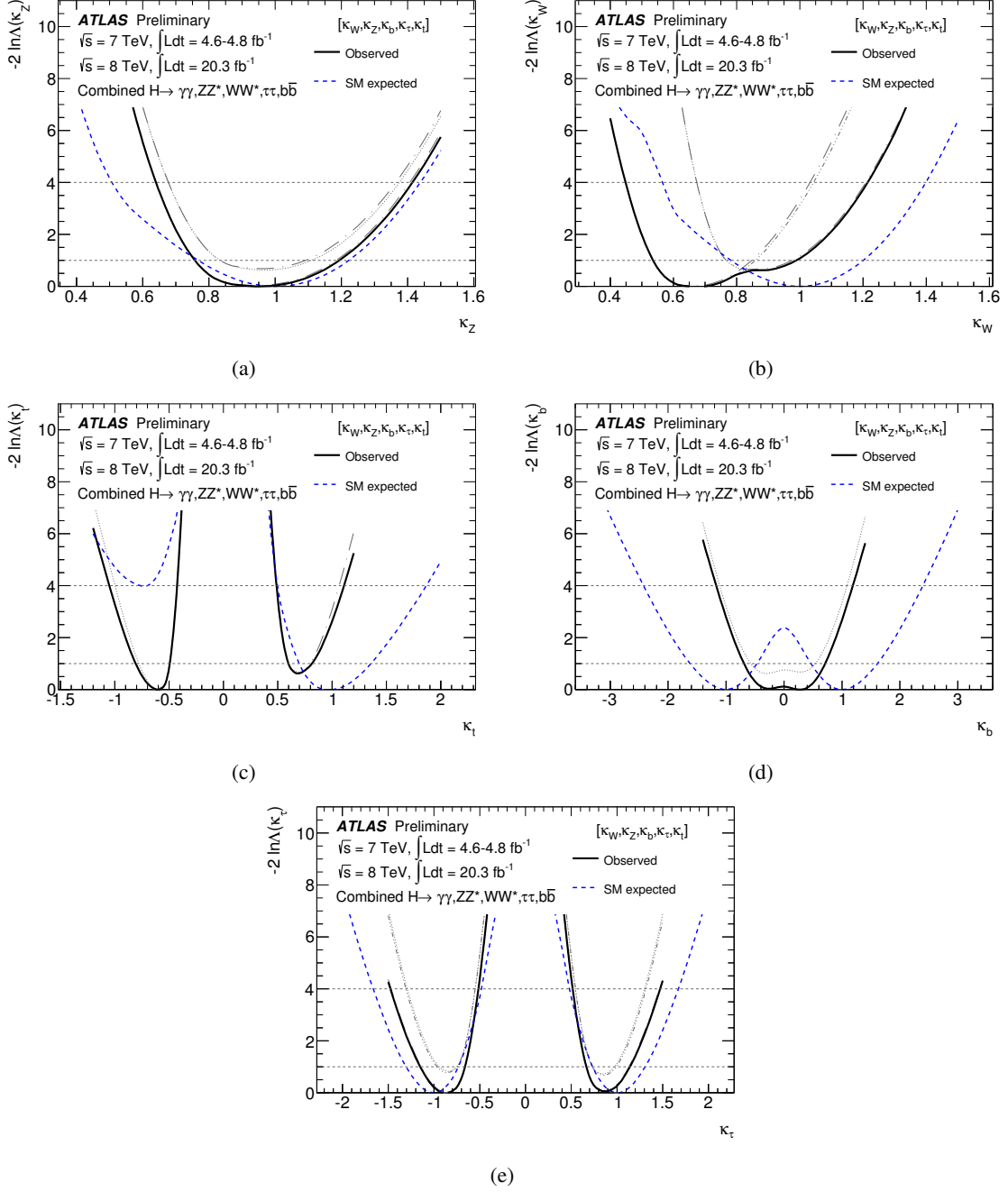
(a)

(b)

(c)

(d)

(e)

Figure 12: Results of fits for the generic model 1: only SM particles in loops and total width fixed to SM value. Each figure shows the likelihood curve for the relevant parameter, with all the other parameters profiled. The dashed curves show the SM expectations. The thin dotted and dash-dotted lines indicate the continuations of the likelihood curves when restricting the other parameters to either their positive or negative sector.

Hence only positive values for all κ-factors are shown without loss of generality. The ratio λ_{tg} is not constrained by the fit, since the Higgs-top coupling only comes from the $gg \to H$ process and is degenerate with the effective Higgs-gluon coupling. This could be improved with an observation of the ttH channel, which would independently probe the Higgs-top coupling. The seven-dimensional compatibility of the SM hypothesis with the best-fit point is 21%. The corresponding fitted values of the couplings ratios can be found in Fig. 14(b).

5.6.3 Summary

The generic coupling fits allow potential deviations from the SM hypothesis to be searched for, without assumptions on the relationships between the coupling scale factors. For a better overview, both measurements are summarised in Figure 14.

For the measurements in the first generic model, it should be noted that the low fitted value of κ_b causes a reduction of the total width Γ_H by approximately a factor of two compared to the SM expectation (see Eq. 5), which in turn induces a reduction of all other κ-values by an approximate factor $\sqrt{2}$. This factor drops out for λ values which are ratios of κ's. Taking this correlated effect into account, the measurement is in agreement with the SM expectation.

The fit in the second generic benchmark model uses only the basic assumptions as stated at the beginning of this Section and hence represents the most model-independent determination of coupling scale factors that is currently possible. Hence the measurement of the ratio λ_{WZ} from this benchmark model can be seen as a generalised version of the measurement in Section 5.3, using less assumptions but also giving a slightly worse expected precision. All results of this fit are in good agreement with the SM expectation.

6   Conclusions

An update of the determination of the couplings of the Higgs boson is presented, using pp collision data corresponding to an integrated luminosity of up to 4.8 fb^{-1} at $\sqrt{s} = 7$ TeV and 20.3 fb^{-1} at $\sqrt{s} = 8$ TeV for the $H \to \gamma\gamma$, $H \to ZZ^* \to 4\ell$, $H \to WW^* \to \ell\nu\ell\nu$ and $H \to b\bar{b}$ channels, and 20.3 fb^{-1} at $\sqrt{s} = 8$ TeV for the $H \to \tau\tau$ channel. The combined measurement of the global signal strength results in a value of $1.30 \pm 0.12 \,(\text{stat}) \,^{+0.14}_{-0.11} \,(\text{sys})$ obtained at the mass of 125.5 GeV. The combination of the $H \to b\bar{b}$ and $H \to \tau\tau$ channels provides evidence for direct fermion decays at the 3.7σ level, with a signal strength of $\mu^{bb,\tau\tau} = 1.09 \pm 0.24 \,(\text{stat}) \,^{+0.27}_{-0.21} \,(\text{sys})$.

The cross section ratio between vector boson-mediated and gluon- (top-) initiated Higgs boson production processes is determined to be $\mu_{\text{VBF+VH}}/\mu_{\text{ggF+}ttH} = 1.4^{+0.5}_{-0.4} \,(\text{stat}) \,^{+0.4}_{-0.2} \,(\text{sys})$. A determination of $\mu_{\text{VBF}}/\mu_{\text{ggF+}ttH}$ provides evidence for VBF production at the 4.1σ level.

The compatibility of the measured yields for the studied channels with the predictions for the SM Higgs boson is tested under various benchmark assumptions probing salient features of the couplings. A summary of coupling scale factor measurements in all benchmark models is shown in Fig. 15. Beyond the Standard Model contributions are also probed, in the effective coupling of the Higgs boson to photons and gluons, and as a branching ratio to invisible or undetected decay modes, for which an upper limit is set at $\text{BR}_{\text{i.,u.}} < 0.41$ (95% CL). Finally, generic models are explored, which feature independent couplings to the particles accessible with the current data, without and with possible BSM contributions in the loops.

Compatibility with the SM is found in all the tests performed, with probabilities ranging from 7% to 21%.
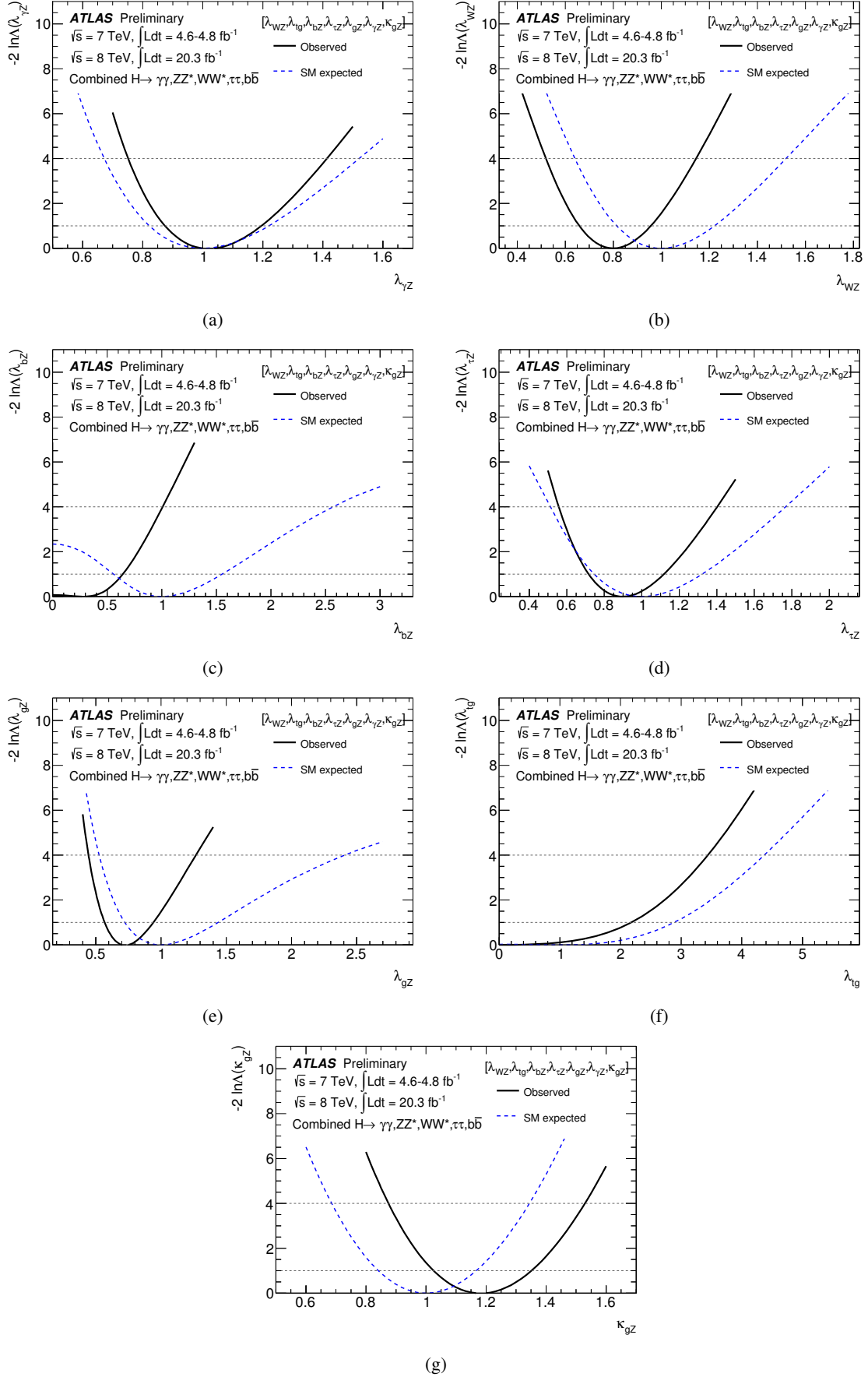
Figure 13: Results of fits for the generic model 222 independent κ_γ, κ_g and no assumption on the total width. Each figure shows the likelihood curve for the relevant parameter, with all the other parameters profiled. The dashed curves show the SM expectations.
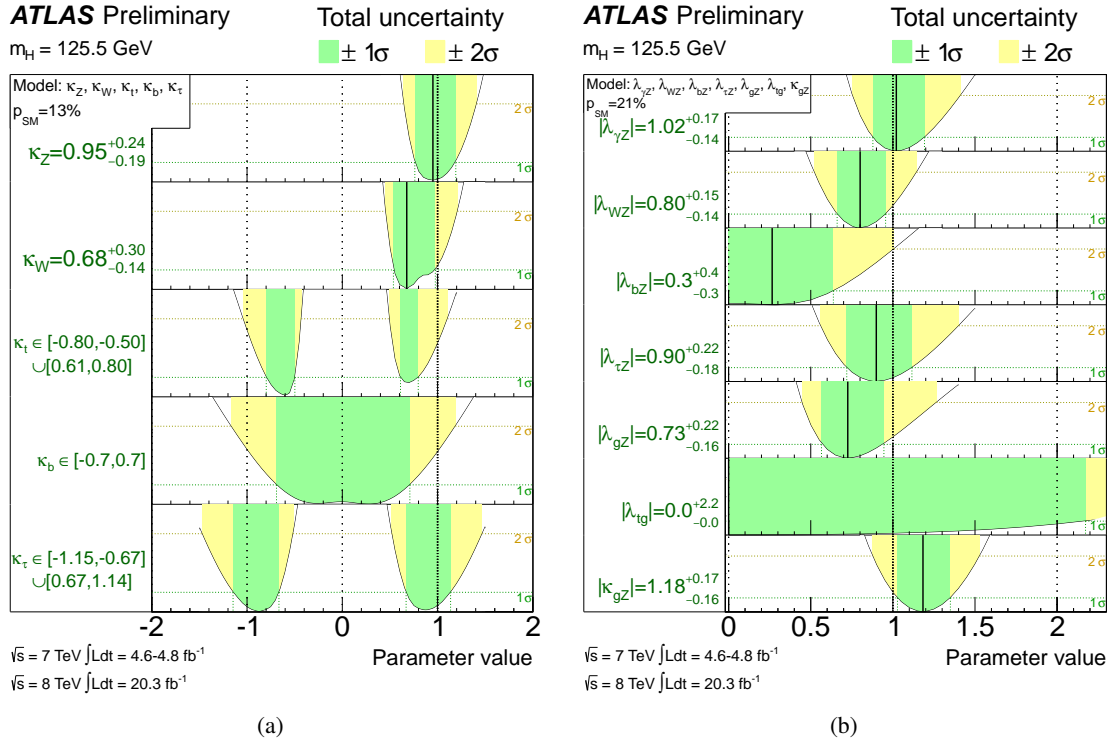
Figure 14: Summary of the coupling scale factor measurements in the generic models discussed in Section 5.6: a) generic model 1, only SM particles; b) generic model 2, independent κ_γ, κ_g and no assumption on the total width. The best-fit values are represented by the solid vertical lines, with the total $\pm 1\sigma$ and $\pm 2\sigma$ uncertainties indicated by the green and yellow shaded bands, respectively. For each model the n-dimensional compatibility of the SM hypothesis with the best-fit point is given by p_{SM}.
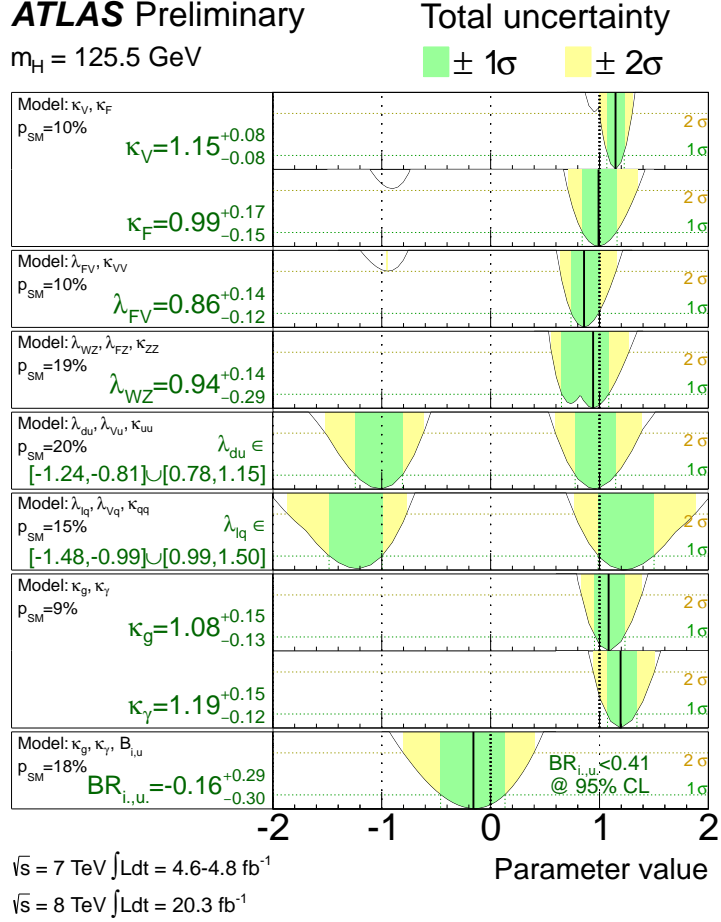
Figure 15: Summary of the coupling scale factor measurements for $m_H = 125.5$ GeV. The best-fit values are represented by the solid black vertical lines. The measurements in the different benchmark models, separated by double lines in the figure, are strongly correlated, as they are obtained from fits to the same experimental data. Hence, they should not be considered as independent measurements and an overall χ^2-like compatibility test to the SM is not possible. For each model the n-dimensional compatibility of the SM hypothesis with the best fit point is given by p_{SM}.

References

[1] ATLAS Collaboration, *Observation of a new particle in the search for the Standard Model Higgs boson with the ATLAS detector at the LHC*, Phys. Lett. **B 716** (2012) 1, `arXiv:1207.7214` `[hep-ex]`.

[2] CMS Collaboration, *Observation of a new boson at a mass of 125 GeV with the CMS experiment at the LHC*, Phys. Lett. **B 716** (2012) 30, `arXiv:1207.7235 [hep-ex]`.

[3] ATLAS Collaboration, *Measurements of Higgs boson production and couplings in diboson final states with the ATLAS detector at the LHC*, Phys. Lett. **B 726** (2013) 88, `arXiv:1307.1427` `[hep-ex]`.

[4] CMS Collaboration, *Evidence for the direct decay of the 125 GeV Higgs boson to fermions*, `arXiv:1401.6527 [hep-ex]`.

[5] ATLAS Collaboration, *Search for the bb decay of the Standard Model Higgs boson in associated W/ZH production with the ATLAS detector*, ATLAS-CONF-2013-079 (2013). `https://cds.cern.ch/record/1563235`.

[6] ATLAS Collaboration, *Evidence for Higgs Boson Decays to the $\tau^+\tau^-$ Final State with the ATLAS Detector*, ATLAS-CONF-2013-108 (2013). `https://cds.cern.ch/record/1632191`.

[7] ATLAS Collaboration, *Improved luminosity determination in pp collisions at $\sqrt{s}$ = 7 TeV using the ATLAS detector at the LHC*, Eur. Phys. J. **C 73** (2013) 2518, `arXiv:1302.4393 [hep-ex]`.

[8] ATLAS Collaboration, *Combined search for the Standard Model Higgs boson in pp collisions at $\sqrt{s}$=7 TeV with the ATLAS detector*, Phys. Rev. **D 86** (2012) 032003, `arXiv:1207.0319 [hep-ex]`.

[9] ATLAS and CMS Collaborations, *Procedure for the LHC Higgs boson search combination in Summer 2011*, ATL-PHYS-PUB-2011-011, CERN-CMS-NOTE-2011-005 (2011). `http://cdsweb.cern.ch/record/1375842`.

[10] L. Moneta, K. Belasco, K. S. Cranmer, S. Kreiss, A. Lazzaro, et al., *The RooStats Project*, PoS **ACAT2010** (2010) 057, `arXiv:1009.1003 [physics.data-an]`.

[11] K. Cranmer, G. Lewis, L. Moneta, A. Shibata, and W. Verkerke, *HistFactory: A tool for creating statistical models for use with RooFit and RooStats*, CERN-OPEN-2012-016 (2012). `http://cdsweb.cern.ch/record/1456844`.

[12] W. Verkerke and D. Kirkby, *The RooFit toolkit for data modelling*, `arXiv:physics/0306116v1 [physics.data-an]`.

[13] G. Cowan, K. Cranmer, E. Gross, and O. Vitells, *Asymptotic formulae for likelihood-based tests of new physics*, Eur. Phys. J. **C 71** (2011) 1554, `arXiv:1007.1727 [physics.data-an]`.

[14] LHC Higgs Cross Section Working Group, S. Heinemeyer, C. Mariotti, G. Passarino, and R. Tanaka (Eds.), *Handbook of LHC Higgs Cross Sections: 3. Higgs Properties*, `arXiv:1307.1347 [hep-ph]`.

[15] ATLAS Collaboration, *Evidence for the spin-0 nature of the Higgs boson using ATLAS data*, Phys. Lett. **B 726** (2013) 120, `arXiv:1307.1432 [hep-ex]`.

[16] CMS Collaboration, *Measurement of the properties of a Higgs boson in the four-lepton final state*, `arXiv:1312.5353 [hep-ex]`.

[17] ATLAS Collaboration, *Combined coupling measurements of the Higgs-like boson with the ATLAS detector using up to 25 fb^{-1} of proton-proton collision data*, ATLAS-CONF-2013-034 (2013). `https://cds.cern.ch/record/1528170`.

[18] ALEPH Collaboration, CDF Collaboration, D0 Collaboration, DELPHI Collaboration, L3 Collaboration, OPAL Collaboration, SLD Collaboration, LEP Electroweak Working Group, Tevatron Electroweak Working Group, SLD Electroweak and Heavy Flavour Groups Collaboration, *Precision Electroweak Measurements and Constraints on the Standard Model*, `arXiv:1012.2367 [hep-ex]`.

[19] T. Lee, *A Theory of Spontaneous T Violation*, Phys. Rev. **D 8** (1973) 1226.

[20] J. F. Gunion and H. E. Haber, *The CP conserving two Higgs doublet model: The Approach to the decoupling limit*, Phys. Rev. **D 67** (2003) 075019, `arXiv:hep-ph/0207010 [hep-ph]`.

[21] G. Branco et al., *Theory and phenomenology of two-Higgs-doublet models*, Phys. Rept. **516** (2012) 1.

[22] ATLAS Collaboration, *Search for Invisible Decays of a Higgs Boson Produced in Association with a Z Boson in ATLAS*, `arXiv:1402.3244 [hep-ex]`.

[23] LHC Higgs Cross Section Working Group, S. Dittmaier, C. Mariotti, G. Passarino, and R. Tanaka (Eds.), *Handbook of LHC Higgs cross sections: 1. Inclusive observables*, CERN-2011-002 (CERN, Geneva, 2011), `arXiv:1101.0593 [hep-ph]`.

A   Appendix: Coupling scale factor relations for the dominant channels

For each model considered in the note, the formulae below give the scaling properties of the most relevant Higgs boson production cross sections and branching ratios, with the elementary couplings (relative to SM ones). In some of the fits, κ_H and the effective scale factors κ_γ and κ_g for the loop-induced $H \to \gamma\gamma$ and $gg \to H$ processes are expressed as a function of the more fundamental factors κ_W, κ_Z, κ_t, κ_b and κ_τ (only the dominant fermion contributions are indicated here for simplicity). The relevant relationships are:

$$\kappa_g^2(\kappa_b, \kappa_t) \quad = \quad \frac{\kappa_t^2 \cdot \sigma_{ggH}^{tt} + \kappa_b^2 \cdot \sigma_{ggH}^{bb} + \kappa_t \kappa_b \cdot \sigma_{ggH}^{tb}}{\sigma_{ggH}^{tt} + \sigma_{ggH}^{bb} + \sigma_{ggH}^{tb}} \tag{6}$$

$$\kappa_{VBF}^2(\kappa_W, \kappa_Z) \quad = \quad \frac{\kappa_W^2 \cdot \sigma_{VBF}^{WW} + \kappa_Z^2 \cdot \sigma_{VBF}^{ZZ}}{\sigma_{VBF}^{WW} + \sigma_{VBF}^{ZZ}} \tag{7}$$

$$\kappa_\gamma^2(\kappa_b, \kappa_t, \kappa_\tau, \kappa_W) \quad = \quad \frac{\sum_{i,j} \kappa_i \kappa_j \cdot \Gamma_{\gamma\gamma}^{ij}}{\sum_{i,j} \Gamma_{\gamma\gamma}^{ij}} \tag{8}$$

$$\kappa_H^2(\kappa_j) \quad = \quad \sum_{\substack{jj=WW^*,\, ZZ^*,\, b\bar{b},\, \tau^-\tau^+, \\ \gamma\gamma,\, Z\gamma,\, gg,\, t\bar{t},\, c\bar{c},\, s\bar{s},\, \mu^-\mu^+}} \frac{\kappa_j^2 \Gamma_{jj}^{SM}}{\Gamma_H^{SM}}, \tag{9}$$

where σ_{ggH}^{ij}, σ_{VBF}^{ii}, $\Gamma_{\gamma\gamma}^{ij}$ and Γ_{ff}^{SM} are obtained from theory [14, 23].

A.1   Fermion versus vector couplings

A.1.1   Only SM contributions to the total width

$$\sigma(gg \to H) * \mathrm{BR}(H \to \gamma\gamma) \quad \sim \quad \frac{\kappa_F^2 \cdot \kappa_\gamma^2(\kappa_F, \kappa_F, \kappa_F, \kappa_V)}{0.75 \cdot \kappa_F^2 + 0.25 \cdot \kappa_V^2}$$

$$\sigma(qq' \to qq'H) * \mathrm{BR}(H \to \gamma\gamma) \quad \sim \quad \frac{\kappa_V^2 \cdot \kappa_\gamma^2(\kappa_F, \kappa_F, \kappa_F, \kappa_V)}{0.75 \cdot \kappa_F^2 + 0.25 \cdot \kappa_V^2}$$

$$\sigma(gg \to H) * \mathrm{BR}(H \to ZZ^*, H \to WW^*) \quad \sim \quad \frac{\kappa_F^2 \cdot \kappa_V^2}{0.75 \cdot \kappa_F^2 + 0.25 \cdot \kappa_V^2} \tag{10}$$

$$\sigma(qq' \to qq'H) * \mathrm{BR}(H \to ZZ^*, H \to WW^*) \quad \sim \quad \frac{\kappa_V^2 \cdot \kappa_V^2}{0.75 \cdot \kappa_F^2 + 0.25 \cdot \kappa_V^2}$$

$$\sigma(qq' \to qq'H, VH) * \mathrm{BR}(H \to \tau\tau, H \to b\bar{b}) \quad \sim \quad \frac{\kappa_V^2 \cdot \kappa_F^2}{0.75 \cdot \kappa_F^2 + 0.25 \cdot \kappa_V^2},$$

where $\kappa_\gamma(\kappa_F, \kappa_F, \kappa_V, \kappa_V)$ is the SM functional dependence of the effective scale factor κ_γ on the scale factors κ_F and κ_V, which is to first approximation:[8]

$$\kappa_\gamma^2(\kappa_F, \kappa_F, \kappa_F, \kappa_V) = 1.59 \cdot \kappa_V^2 - 0.66 \cdot \kappa_V \kappa_F + 0.07 \cdot \kappa_F^2. \tag{11}$$

---

[8] The fit uses the full dependence of κ_γ on κ_W, κ_t, κ_b and κ_τ [14].

The denominator is the total width scale factor κ_H^2 expressed as a function of the scale factors κ_F and κ_V, where 0.75 is the SM branching ratio to fermion and gluon final states and 0.25 the SM branching ratio into WW^*, ZZ^* and $\gamma\gamma$ for $m_H = 125.5\,\mathrm{GeV}$.

A.1.2 No assumption on the total width

$$
\begin{aligned}
\sigma(gg \to H) * \mathrm{BR}(H \to \gamma\gamma) &\sim \lambda_{FV}^2 \cdot \kappa_{VV}^2 \cdot \kappa_\gamma^2(\lambda_{FV}, \lambda_{FV}, \lambda_{FV}, 1) \\
\sigma(qq' \to qq'H) * \mathrm{BR}(H \to \gamma\gamma) &\sim \kappa_{VV}^2 \cdot \kappa_\gamma^2(\lambda_{FV}, \lambda_{FV}, \lambda_{FV}, 1) \\
\sigma(gg \to H) * \mathrm{BR}(H \to ZZ^*, H \to WW^*) &\sim \lambda_{FV}^2 \cdot \kappa_{VV}^2 \\
\sigma(qq' \to qq'H) * \mathrm{BR}(H \to ZZ^*, H \to WW^*) &\sim \kappa_{VV}^2 \\
\sigma(qq' \to qq'H, VH) * \mathrm{BR}(H \to \tau\tau, H \to b\bar{b}) &\sim \kappa_{VV}^2 \cdot \lambda_{FV}^2,
\end{aligned}
\tag{12}
$$

where the second order polynomial form of $\kappa_\gamma^2(\kappa_F, \kappa_F, \kappa_F, \kappa_V)$, given in Equations 8, 11, allows to factorize out the scale factor κ_V into the common factor κ_{VV} and the ratio λ_{FV}.

A.2 Probing the custodial symmetry of the W and Z couplings

$$
\begin{aligned}
\sigma(gg \to H) * \mathrm{BR}(H \to \gamma\gamma) &\sim \lambda_{FZ}^2 \cdot \kappa_{ZZ}^2 \cdot \kappa_\gamma^2(\lambda_{FZ}, \lambda_{FZ}, \lambda_{FZ}, \lambda_{WZ}) \\
\sigma(qq' \to qq'H) * \mathrm{BR}(H \to \gamma\gamma) &\sim \kappa_{VBF}^2(\lambda_{WZ}, 1) \cdot \kappa_{ZZ}^2 \cdot \kappa_\gamma^2(\lambda_{FZ}, \lambda_{FZ}, \lambda_{FZ}, \lambda_{WZ}) \\
\sigma(gg \to H) * \mathrm{BR}(H \to ZZ^*) &\sim \lambda_{FZ}^2 \cdot \kappa_{ZZ}^2 \\
\sigma(qq' \to qq'H) * \mathrm{BR}(H \to ZZ^*) &\sim \kappa_{VBF}^2(\lambda_{WZ}, 1) \cdot \kappa_{ZZ}^2 \\
\sigma(gg \to H) * \mathrm{BR}(H \to WW^*) &\sim \lambda_{FZ}^2 \cdot \kappa_{ZZ}^2 \cdot \lambda_{WZ}^2 \\
\sigma(qq' \to qq'H) * \mathrm{BR}(H \to WW^*) &\sim \kappa_{VBF}^2(\lambda_{WZ}, 1) \cdot \kappa_{ZZ}^2 \cdot \lambda_{WZ}^2 \\
\sigma(qq' \to qq'H) * \mathrm{BR}(H \to \tau\tau) &\sim \kappa_{VBF}^2(\lambda_{WZ}, 1) \cdot \kappa_{ZZ}^2 \cdot \lambda_{FZ}^2,
\end{aligned}
\tag{13}
$$

where $\kappa_{VBF}^2(\kappa_W, \kappa_Z)$ is the second order polynomial functional dependence of the VBF cross section on the coupling scale factors κ_W and κ_Z.

A.3 Probing relations within the fermion coupling sector

A.3.1 Probing the up- and down-type fermion symmetry

$$
\begin{aligned}
\sigma(gg \to H) * \mathrm{BR}(H \to \gamma\gamma) &\sim \kappa_g^2(\lambda_{du}, 1) \cdot \kappa_{uu}^2 \cdot \kappa_\gamma^2(\lambda_{du}, 1, \lambda_{du}, \lambda_{Vu}) \\
\sigma(qq' \to qq'H) * \mathrm{BR}(H \to \gamma\gamma) &\sim \lambda_{Vu}^2 \cdot \kappa_{uu}^2 \cdot \kappa_\gamma^2(\lambda_{du}, 1, \lambda_{du}, \lambda_{Vu}) \\
\sigma(gg \to H) * \mathrm{BR}(H \to ZZ^*, H \to WW^*) &\sim \kappa_g^2(\lambda_{du}, 1) \cdot \kappa_{uu}^2 \cdot \lambda_{Vu}^2 \\
\sigma(qq' \to qq'H) * \mathrm{BR}(H \to ZZ^*, H \to WW^*) &\sim \lambda_{Vu}^2 \cdot \kappa_{uu}^2 \cdot \lambda_{Vu}^2 \\
\sigma(gg \to H) * \mathrm{BR}(H \to \tau\tau) &\sim \kappa_g^2(\lambda_{du}, 1) \cdot \kappa_{uu}^2 \cdot \lambda_{du}^2 \\
\sigma(qq' \to qq'H, VH) * \mathrm{BR}(H \to \tau\tau, H \to b\bar{b}) &\sim \lambda_{Vu}^2 \cdot \kappa_{uu}^2 \cdot \lambda_{du}^2,
\end{aligned}
\tag{14}
$$

A.3.2 Probing the quark and lepton symmetry

$$\sigma(gg \to H) * \mathrm{BR}(H \to \gamma\gamma) \quad \sim \quad \kappa_{qq}^2 \cdot \kappa_\gamma^2(1, 1, \lambda_{lq}, \lambda_{Vq})$$

$$\sigma(qq' \to qq'H) * \mathrm{BR}(H \to \gamma\gamma) \quad \sim \quad \lambda_{Vq}^2 \cdot \kappa_{qq}^2 \cdot \kappa_\gamma^2(1, 1, \lambda_{lq}, \lambda_{Vq})$$

$$\sigma(gg \to H) * \mathrm{BR}(H \to ZZ^*, H \to WW^*) \quad \sim \quad \kappa_{qq}^2 \cdot \lambda_{Vq}^2$$

$$\sigma(qq' \to qq'H) * \mathrm{BR}(H \to ZZ^*, H \to WW^*) \quad \sim \quad \lambda_{Vq}^2 \cdot \kappa_{qq}^2 \cdot \lambda_{Vq}^2 \tag{15}$$

$$\sigma(gg \to H) * \mathrm{BR}(H \to \tau\tau) \quad \sim \quad \kappa_{qq}^2 \cdot \lambda_{lq}^2$$

$$\sigma(qq' \to qq'H, VH) * \mathrm{BR}(H \to \tau\tau) \quad \sim \quad \lambda_{Vq}^2 \cdot \kappa_{qq}^2 \cdot \lambda_{lq}^2$$

$$\sigma(qq' \to qq'H, VH) * \mathrm{BR}(H \to b\bar{b}) \quad \sim \quad \lambda_{Vq}^2 \cdot \kappa_{qq}^2,$$

A.4 Probing beyond the SM contributions

A.4.1 Only SM contributions to the total width

$$\sigma(gg \to H) * \mathrm{BR}(H \to \gamma\gamma) \quad \sim \quad \frac{\kappa_g^2 \cdot \kappa_\gamma^2}{0.085 \cdot \kappa_g^2 + 0.0023 \cdot \kappa_\gamma^2 + 0.91}$$

$$\sigma(qq' \to qq'H) * \mathrm{BR}(H \to \gamma\gamma) \quad \sim \quad \frac{\kappa_\gamma^2}{0.085 \cdot \kappa_g^2 + 0.0023 \cdot \kappa_\gamma^2 + 0.91}$$

$$\sigma(gg \to H) * \mathrm{BR}(H \to ZZ^*, H \to WW^*) \quad \sim \quad \frac{\kappa_g^2}{0.085 \cdot \kappa_g^2 + 0.0023 \cdot \kappa_\gamma^2 + 0.91} \tag{16}$$

$$\sigma(qq' \to qq'H) * \mathrm{BR}(H \to ZZ^*, H \to WW^*) \quad \sim \quad \frac{1}{0.085 \cdot \kappa_g^2 + 0.0023 \cdot \kappa_\gamma^2 + 0.91}$$

$$\sigma(qq' \to qq'H, VH) * \mathrm{BR}(H \to \tau\tau, H \to b\bar{b}) \quad \sim \quad \frac{1}{0.085 \cdot \kappa_g^2 + 0.0023 \cdot \kappa_\gamma^2 + 0.91}.$$

A.4.2 No assumption on the total width

$$\sigma(gg \to H) * \mathrm{BR}(H \to \gamma\gamma) \quad \sim \quad \frac{\kappa_g^2 \cdot \kappa_\gamma^2}{0.085 \cdot \kappa_g^2 + 0.0023 \cdot \kappa_\gamma^2 + 0.91} \cdot (1 - \mathrm{BR}_{i.,u.})$$

$$\sigma(qq' \to qq'H) * \mathrm{BR}(H \to \gamma\gamma) \quad \sim \quad \frac{\kappa_\gamma^2}{0.085 \cdot \kappa_g^2 + 0.0023 \cdot \kappa_\gamma^2 + 0.91} \cdot (1 - \mathrm{BR}_{i.,u.})$$

$$\sigma(gg \to H) * \mathrm{BR}(H \to ZZ^*, H \to WW^*) \quad \sim \quad \frac{\kappa_g^2}{0.085 \cdot \kappa_g^2 + 0.0023 \cdot \kappa_\gamma^2 + 0.91} \cdot (1 - \mathrm{BR}_{i.,u.}) \tag{17}$$

$$\sigma(qq' \to qq'H) * \mathrm{BR}(H \to ZZ^*, H \to WW^*) \quad \sim \quad \frac{1}{0.085 \cdot \kappa_g^2 + 0.0023 \cdot \kappa_\gamma^2 + 0.91} \cdot (1 - \mathrm{BR}_{i.,u.})$$

$$\sigma(qq' \to qq'H, VH) * \mathrm{BR}(H \to \tau\tau, H \to b\bar{b}) \quad \sim \quad \frac{1}{0.085 \cdot \kappa_g^2 + 0.0023 \cdot \kappa_\gamma^2 + 0.91} \cdot (1 - \mathrm{BR}_{i.,u.}).$$

A.5 Generic models

A.5.1 Generic model 1: only SM particles in loops and the total width

$$
\begin{aligned}
\sigma(gg \to H) * \mathrm{BR}(H \to \gamma\gamma) &\sim \frac{\kappa_g^2(\kappa_b, \kappa_t) \cdot \kappa_\gamma^2(\kappa_b, \kappa_t, \kappa_\tau, \kappa_W)}{\kappa_H^2(\kappa_b, \kappa_t, \kappa_\tau, \kappa_W, \kappa_Z)} \\[1em]
\sigma(qq' \to qq'H) * \mathrm{BR}(H \to \gamma\gamma) &\sim \frac{\kappa_{\mathrm{VBF}}^2(\kappa_W, \kappa_Z) \cdot \kappa_\gamma^2(\kappa_b, \kappa_t, \kappa_\tau, \kappa_W)}{\kappa_H^2(\kappa_b, \kappa_t, \kappa_\tau, \kappa_W, \kappa_Z)} \\[1em]
\sigma(gg \to H) * \mathrm{BR}(H \to ZZ^*) &\sim \frac{\kappa_g^2(\kappa_b, \kappa_t) \cdot \kappa_Z^2}{\kappa_H^2(\kappa_b, \kappa_t, \kappa_\tau, \kappa_W, \kappa_Z)} \\[1em]
\sigma(qq' \to qq'H) * \mathrm{BR}(H \to ZZ^*) &\sim \frac{\kappa_{\mathrm{VBF}}^2(\kappa_W, \kappa_Z) \cdot \kappa_Z^2}{\kappa_H^2(\kappa_b, \kappa_t, \kappa_\tau, \kappa_W, \kappa_Z)} \\[1em]
\sigma(gg \to H) * \mathrm{BR}(H \to WW^*) &\sim \frac{\kappa_g^2(\kappa_b, \kappa_t) \cdot \kappa_W^2}{\kappa_H^2(\kappa_b, \kappa_t, \kappa_\tau, \kappa_W, \kappa_Z)} \\[1em]
\sigma(qq' \to qq'H) * \mathrm{BR}(H \to WW^*) &\sim \frac{\kappa_{\mathrm{VBF}}^2(\kappa_W, \kappa_Z) \cdot \kappa_W^2}{\kappa_H^2(\kappa_b, \kappa_t, \kappa_\tau, \kappa_W, \kappa_Z)} \\[1em]
\sigma(gg \to H) * \mathrm{BR}(H \to \tau\tau) &\sim \frac{\kappa_g^2(\kappa_b, \kappa_t) \cdot \kappa_\tau^2}{\kappa_H^2(\kappa_b, \kappa_t, \kappa_\tau, \kappa_W, \kappa_Z)} \\[1em]
\sigma(qq' \to qq'H) * \mathrm{BR}(H \to \tau\tau) &\sim \frac{\kappa_{\mathrm{VBF}}^2(\kappa_W, \kappa_Z) \cdot \kappa_\tau^2}{\kappa_H^2(\kappa_b, \kappa_t, \kappa_\tau, \kappa_W, \kappa_Z)} \\[1em]
\sigma(WH) * \mathrm{BR}(H \to b\bar{b}) &\sim \frac{\kappa_W^2 \cdot \kappa_b^2}{\kappa_H^2(\kappa_b, \kappa_t, \kappa_\tau, \kappa_W, \kappa_Z)} \\[1em]
\sigma(ZH) * \mathrm{BR}(H \to b\bar{b}) &\sim \frac{\kappa_Z^2 \cdot \kappa_b^2}{\kappa_H^2(\kappa_b, \kappa_t, \kappa_\tau, \kappa_W, \kappa_Z)},
\end{aligned}
\tag{18}
$$

A.5.2 Generic Model 2: allowing deviations in loop couplings and the total width

$$
\begin{aligned}
\sigma(gg \to H) * \mathrm{BR}(H \to \gamma\gamma) &\sim \kappa_{gZ}^2 \cdot \lambda_{\gamma Z}^2 \\
\sigma(qq' \to qq'H) * \mathrm{BR}(H \to \gamma\gamma) &\sim \kappa_{\mathrm{VBF}}^2(\lambda_{WZ}, 1)/\lambda_{gZ}^2 \cdot \kappa_{gZ}^2 \cdot \lambda_{\gamma Z}^2 \\
\sigma(gg \to H) * \mathrm{BR}(H \to ZZ^*) &\sim \kappa_{gZ}^2 \\
\sigma(qq' \to qq'H) * \mathrm{BR}(H \to ZZ^*) &\sim \kappa_{\mathrm{VBF}}^2(\lambda_{WZ}, 1)/\lambda_{gZ}^2 \cdot \kappa_{gZ}^2 \\
\sigma(gg \to H) * \mathrm{BR}(H \to WW^*) &\sim \kappa_{gZ}^2 \cdot \lambda_{WZ}^2 \\
\sigma(qq' \to qq'H) * \mathrm{BR}(H \to WW^*) &\sim \kappa_{\mathrm{VBF}}^2(\lambda_{WZ}, 1)/\lambda_{gZ}^2 \cdot \kappa_{gZ}^2 \cdot \lambda_{WZ}^2 \\
\sigma(gg \to H) * \mathrm{BR}(H \to \tau\tau) &\sim \kappa_{gZ}^2 \cdot \lambda_{\tau Z}^2 \\
\sigma(qq' \to qq'H) * \mathrm{BR}(H \to \tau\tau) &\sim \kappa_{\mathrm{VBF}}^2(\lambda_{WZ}, 1)/\lambda_{gZ}^2 \cdot \kappa_{gZ}^2 \cdot \lambda_{\tau Z}^2 \\
\sigma(WH) * \mathrm{BR}(H \to b\bar{b}) &\sim \lambda_{WZ}^2/\lambda_{gZ}^2 \cdot \kappa_{gZ}^2 \cdot \lambda_{bZ}^2 \\
\sigma(ZH) * \mathrm{BR}(H \to b\bar{b}) &\sim 1/\lambda_{gZ}^2 \cdot \kappa_{gZ}^2 \cdot \lambda_{bZ}^2,
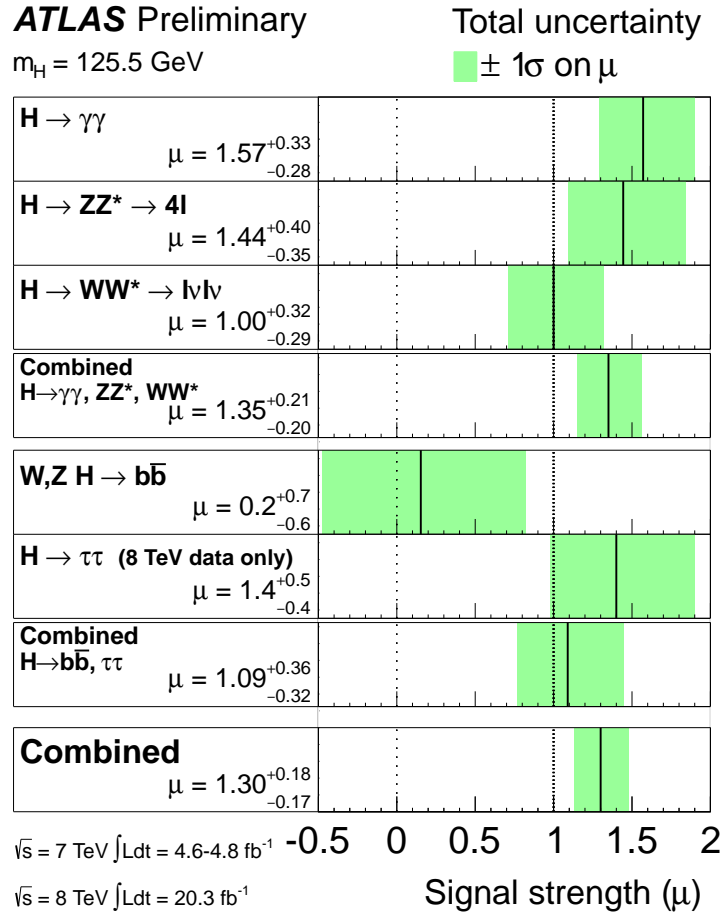\end{aligned}
$$

B Appendix: auxiliary plots

Figure 16: The measured production strengths for a Higgs boson of mass m_H =125.5 GeV, normalised to the SM expectations, for the individual final states and various combinations. The best-fit values are shown by the solid vertical lines. The total $\pm 1\sigma$ uncertainty is indicated by the green shaded band.
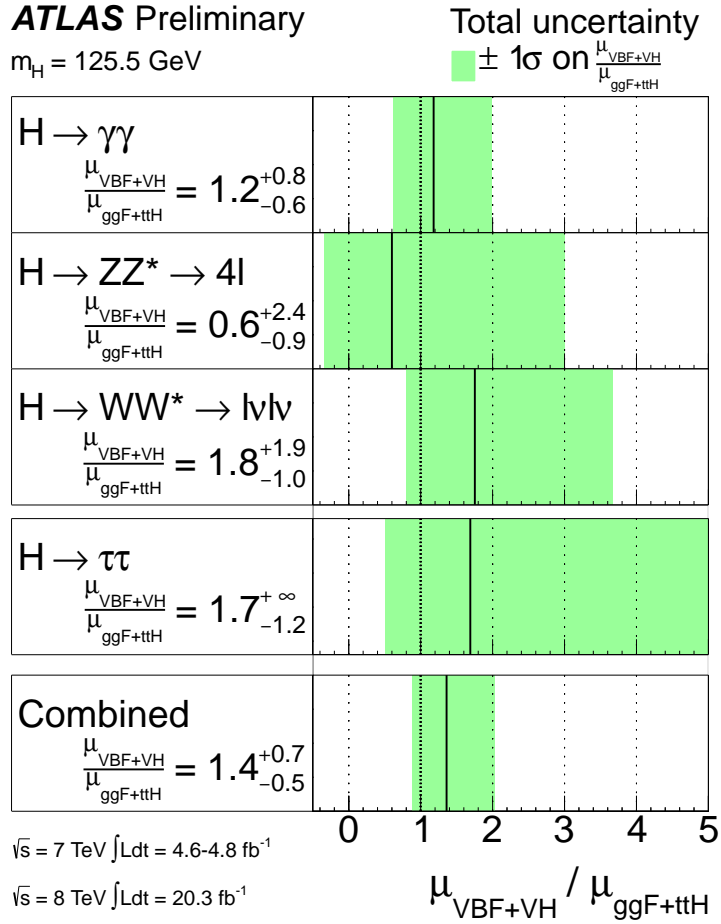
Figure 17: Measurements of the $\mu_{VBF+VH}/\mu_{ggF+ttH}$ ratios for the individual final states and their combination, for a Higgs boson mass m_H =125.5 GeV. The best-fit values are shown by the solid vertical lines. The total $\pm 1\sigma$ uncertainty is indicated by the green shaded band.
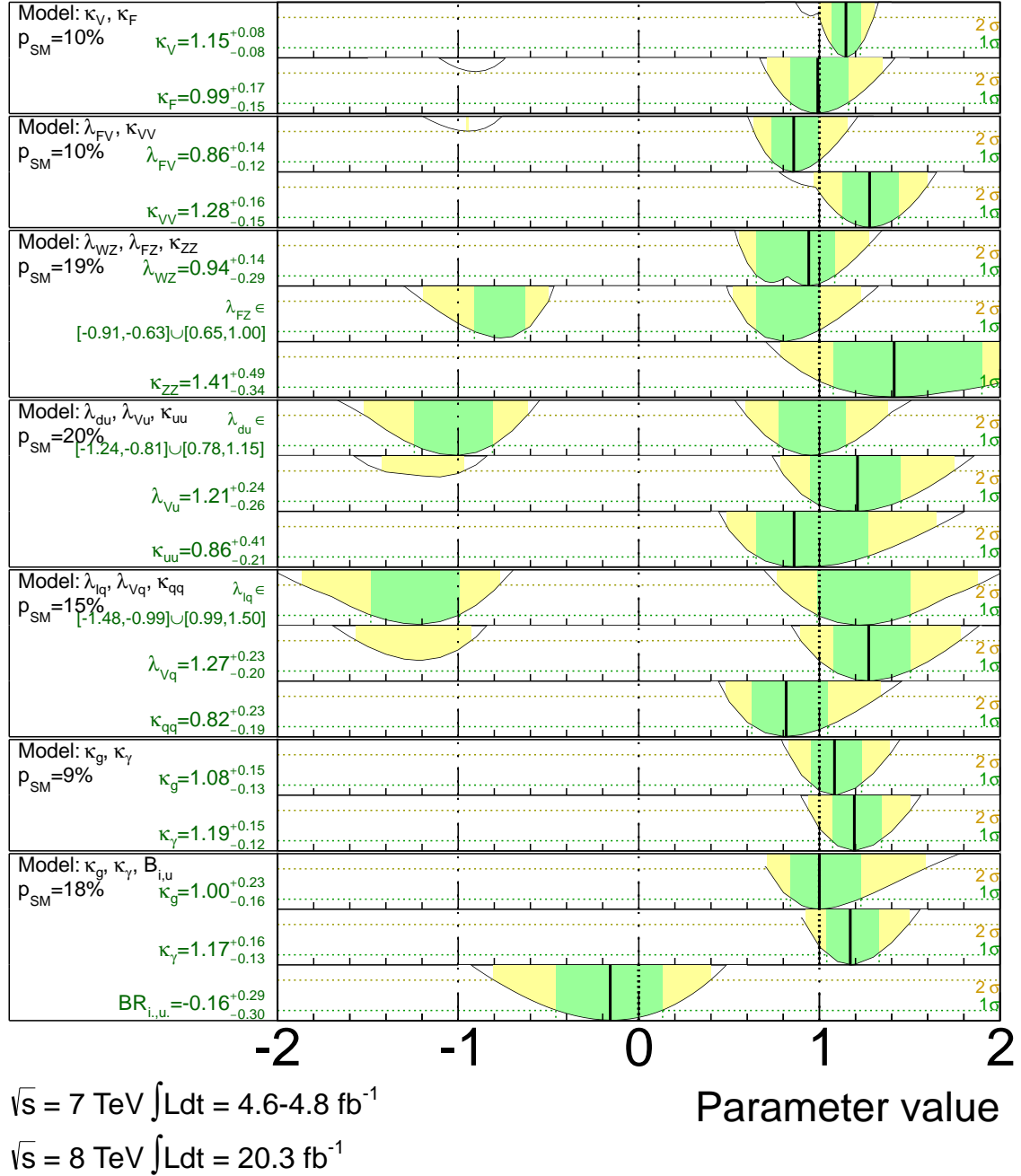
Figure 18: Summary of the coupling scale factor measurements for m_H=125.5 GeV. The best-fit values are represented by the solid black vertical lines. The measurements in the different benchmark models, separated by double lines in the figure, are strongly correlated, as they are obtained from fits to the same experimental data. Hence they should not be considered as independent measurements and an overall χ^2-like compatibility test to the SM is not possible. The values for p_{SM} give for each model the n-dimensional compatibility of the SM hypothesis with the best fit point.